*sustainability*

MDPI

*Article*

# Optimizing Distribution System Resilience in Extreme Weather Using Prosumer-Centric Microgrids with Integrated Distributed Energy Resources and Battery Electric Vehicles

**Muthusamy Thirumalai [1,2], Raju Hariharan [1,*], Thangaraj Yuvaraj [3] and Natarajan Prabaharan [4,*]**

[1] Department of Electrical and Electronics Engineering, Saveetha School of Engineering, Saveetha Institute of Medical and Technical Sciences, Saveetha University, Chennai 602105, India; thirumalai3788@gmail.com
[2] Department of Electronics and Communication Engineering, Saveetha Engineering College, Chennai 602105, India
[3] Centre for Computational Modeling, Chennai Institute of Technology, Chennai 600069, India; yuvaraj4252@gmail.com
[4] School of Electrical and Electronics Engineering, SASTRA Deemed University, Thanjavur 613401, India
* Correspondence: harinov22@gmail.com (R.H.); prabaharan.nataraj@gmail.com (N.P.)

**Abstract:** Electric power networks face vulnerabilities from various hazards, including extreme weather and natural disasters, resulting in prolonged outages and service disruptions. This paper proposes prosumer-centric networked electrical microgrids as a solution. EMGs integrate DERs, like SPV panels, WTs, BESSs, and BEVs, to form autonomous microgrids capable of operating independently during grid disruptions. The SMA was used to identify the appropriate allocation of DERs and BEVs to improve the resilience of the system. Prosumers, acting as both producers and consumers, play a crucial role by generating and sharing electricity within the microgrid. BEVs act as mobile energy storage units during emergencies. Load management and demand response strategies prioritize the energy needs for essential facilities, ensuring uninterrupted operation during adverse weather. Robust communication and control systems improve the emergency coordination and response. The resilience analysis focused on two case studies: moderate and severe damage, both under varying weather conditions. Simulations and experiments assessed the microgrid performance with different levels of DERs and demand. By testing on the IEEE 69-bus RDS, evaluated the EMGs' strengths and limitations, demonstrating their potential to enhance distribution grid resilience against natural disasters.

**Keywords:** battery energy storage systems; distributed energy resources; resilience; networked microgrids; roof-top solar photovoltaic; roof-top wind turbine; battery electric vehicle; radial distribution system



**Citation:** Thirumalai, M.; Hariharan, R.; Yuvaraj, T.; Prabaharan, N. Optimizing Distribution System Resilience in Extreme Weather Using Prosumer-Centric Microgrids with Integrated Distributed Energy Resources and Battery Electric Vehicles. *Sustainability* **2024**, *16*, 2379. https://doi.org/10.3390/su16062379

Academic Editor: Antonio Caggiano

Received: 13 February 2024
Revised: 7 March 2024
Accepted: 8 March 2024
Published: 13 March 2024



## 1. Introduction

The electricity grid is currently experiencing several major issues, ranging from aging infrastructure to expanding cybersecurity and physical security concerns. As infrastructure ages, new threats emerge, including heightened maintenance and operational costs; equipment malfunctions; inefficient operations; and, in severe cases, cascading blackouts [1]. The demand for a consistent electricity supply becomes even more critical during and after extreme events. Previously, events were classified as extreme due to their widespread and severe consequences, as well as their infrequent occurrence [2]. While blackouts are rare events, their socioeconomic costs and consequences are enormous [3]. Over the last few decades, the USA has seen a series of major blackouts, each of which resulted in an estimated USD 1 billion in losses, for a staggering total of more than USD 1 trillion. It is worth mentioning that the vast majority (more than 90%) of these outages have occurred in the power distribution system [4]. The NOAA also reported that the USA experienced

28 confirmed weather and climate disaster events, each causing losses surpassing USD 1 billion in 2023. These events comprised 1 drought, 4 floods, 19 severe storms, 2 tropical cyclones, 1 wildfire, and 1 winter storm. Tragically, these incidents claimed the lives of 492 individuals and had significant economic ramifications for the affected regions. The annual average of such events, adjusted for inflation, from 1980 to 2023 stands at 8.5. However, the recent five-year average (2019–2023) has surged to 20.4 events, indicating a notable increase in frequency and severity [4]. In the ongoing de-carbonization efforts within modern societies, electricity has become increasingly indispensable for sustaining daily operations. Consequently, threats and disruptions to electricity security are escalating and evolving at a pace parallel to advancements in the power grid [5].

The increasing dependence on electricity for essential services underscores the urgent necessity to enhance the resilience of distribution systems against potential threats, like natural disasters. Strengthening these systems is vital to ensuring the continuity of services crucial for healthcare, communication, education, transportation, and emergency response.

These threats have the potential to seriously affect people's quality of life, socioeconomic activity, and national energy security [6]. To address these issues and improve the distribution system resilience, electrical microgrids (EMGs) have emerged as a possible alternative. A microgrid is made up of small-scale distributed energy resources (DERs) that integrate wind energy, solar energy, storage systems, battery electric vehicles (BEVs), and other renewable sources. Microgrids have sparked considerable interest in recent years as a consequence of various research and pilot projects demonstrating their ability to build more radial distribution systems (RDSs) [7].

The use of microgrids provides numerous benefits that considerably improve resilience. For starters, microgrids run autonomously, with the ability to disengage from the main grid in the event of an emergency. This autonomy provides a localized power supply, even during larger system outages, allowing important facilities and communities to keep essential services and operations running during blackouts. Second, microgrids integrate many DERs, resulting in decentralized power generation and less reliance on a single energy source. This diversification strengthens the system's resilience [8]. Furthermore, microgrids improve the load control and demand response, resulting in more efficient energy usage patterns. Microgrids have been further enabled by advancements in communication and control technologies, allowing for enhanced monitoring and management. This real-time control enables dynamic responses to changing conditions, which optimizing energy distribution, reducing losses, and eventually improving the grid reliability [9].

To meet the problems posed by aging infrastructure and possible threats, such as natural catastrophes, it is critical to ensure the resilience of RDSs. Microgrids, with their distributed energy supplies, islanding capability, and modern control systems, provide a promising and sustainable alternative. Integrating microgrids into an RDS offers a solution to bolster resilience, guarantee an uninterrupted power supply, and safeguard critical services and infrastructure during catastrophes. Investing in the creation and deployment of microgrids has the potential to significantly improve our energy future while also benefiting communities and the economy.

## 2. Related Works

Significant research efforts in recent decades have focused on improving the resilience of electricity networks, notably with a focus on DERs. As a result of these efforts, numerous resilience indicators for assessing system performance have been established. The authors utilized a simulation study for AC microgrid formation in an RDS. The simulation results were compared with those of an AC microgrid, affirming the efficacy of the proposed coordinated DC technique for optimizing DER operation. This technique not only enables resilient emergency responses but also enhances economic stability [10].

In the study [11], a novel framework based on the concept of modularity was developed to quantify the resilience of electric distribution networks. Using graph-related theories, a novel path-based approach was proposed to identify possible EMGs and outline their servicing areas. Furthermore, the MG exploration process includes electrical and topological aspects, switching constraints, and reconfiguration choices [11]. The study [12] presented a methodology to quantify the benefits of integrating a solar-based microgrid with electrochemical energy storage in large, non-public office buildings. It evaluated the advantages from both a business perspective and in terms of enhancing energy resilience. The authors created and implemented a method for improving the distribution resilience in large-scale distribution networks. The study [13] presented data to validate the method's primary benefits, including scalability to large-scale systems and the capacity to control uneven AC power flow physics. Additionally, it highlighted a resilient design incorporating hardening, redundancy, and networked microgrids. Notably, the study's findings support the argument that in some scenarios, networked microgrids are the most cost-effective choice [13].

The article [14] suggested an iteration-based linear approximation of the MINLP, with the convergence of the iteration process ensuring its exactness. The efficiency of the devised method was demonstrated by numerical data derived from the IEEE 33- and 69-bus RDSs. The addressed problem involved a software-defined networking-based design that featured a unique event-triggered communication system. This system enabled distributed power sharing among microgrids during both transient and steady-state periods, which is a capability that is currently unattainable with existing technology [15]. The article [16] proposed a technique to ensure microgrid stability by establishing controlled information islands. Unlike traditional control methods, this approach can maintain system operation during information islanding, facilitating load sharing and voltage regulation. This research greatly advanced microgrid technology using RES and its possible impact on the future of RDSs [17].

In reference [18], the researchers established a mathematical methodology to calculate the ideal location and size of DERs. Through a true RDS case study, they showed how their proposed technique enhances system robustness [18]. Optimizing the placement and scale of DGs resulted in significant gains in microgrid network resilience were discussed [19]. The research introduced a two-stage planning technique to enhance the resilience of energy RDSs to storms. This contribution serves as a valuable resource for power systems engineering experts, practitioners, and policymakers, expanding the existing literature on resilience planning [20]. The study [21] outlined a three-stage framework: natural occurrence modeling, component vulnerability assessment, and network resilience enhancement. It evaluated component robustness using fragility models and Monte Carlo simulations, and employed network-hardening strategies, like vegetation control and pole upgrading, to boost the overall resilience.

The study [22] presented a mathematical approach for assessing EMG resilience to HILP windstorms using fragility curves and windstorm profiles to gauge performance decline. Their method is noted for its simplicity and efficiency, facilitating quick understanding and preventive actions [23]. The research strategically analyzed existing approaches, emphasizing resilience-oriented strategies. It then summarized an analytical survey of studies related to using DGs and switches to enhance power distribution system robustness [23]. Furthermore, research [24] focused on analyzing existing strategies, summarizing studies on DGs and switches to bolster power distribution system robustness. It introduced a model that considered DGs, switches, and consumer power patterns during disasters, alongside a novel strategy that integrates transportation networks to enhance resilience [24]. Moreover, ref. [25] introduced a system for optimizing electric bus routing within an RDS to speed up restoration. Their proposed model considers trip duration, bus capacity, and electricity usage, offering the potential to significantly improve recovery efforts' efficiency.

The study [22] provided a mathematical approach for evaluating EMG resilience in the face of high-impact, low-probability windstorms. The framework used overhead distribution branch fragility curves and the windstorm profile at the same time to measure the decrease in EMG performance, specifically in terms of the provided load. The suggested analytical method is distinguished by its simplicity and computational efficiency, allowing for a quick way of understanding the unfavorable effects of an impending windstorm and taking appropriate preventive steps [22]. The research focused on a strategic analysis of several existing strategies, with an emphasis on resiliency-oriented approaches. Following this, an attempt was made to summarize an analytical survey of existing studies linked to the use of DGs and switches to improve power distribution system robustness. The study developed an intriguing model for resiliency that took into account DGs, switches, and consumer power consumption patterns during natural disasters. To address this, the researchers developed a novel strategy for boosting power RDS resilience through transportation network integration [24]. Their findings can help both researchers and practitioners create more resilient and efficient power system recovery systems [24]. The article's main result was the development of a system for optimizing the routing and scheduling of electric buses within an RDS in order to speed up the restoration process. The authors suggested a mixed-integer linear programming model that took into account variables including the trip duration, bus capacity, and electricity usage in different places [25]. This technology has the potential to significantly increase the efficiency and effectiveness of power system recovery efforts.

Electric power networks face vulnerabilities from a multitude of hazards, such as extreme weather events, natural disasters, equipment failures, and deliberate attacks [26–28]. These hazards lead to power outages, service disruptions, and economic losses. The subsequent explanations provide a detailed discussion of their drawbacks on electric power networks influenced by a variety of hazards. Extreme weather events, like hurricanes and storms, can damage power infrastructure, causing widespread outages and lengthy restoration times [26], while equipment failures, such as transformer malfunctions and line faults, contribute to unplanned interruptions, affecting residential and commercial consumers [27]. Deliberate attacks on power grids, such as cyber-attacks and physical sabotage, pose security risks and threaten national security and public safety [28]. The reliance on centralized power generation sources increases vulnerabilities, heightening the risk of cascading blackouts during emergencies [27,28]. Enhancing the resilience of electric power networks is crucial to mitigating these impacts and ensuring a reliable energy supply for communities and industries.

Despite previous research that addressed power distribution system resilience, significant gaps persist in generating realistic case studies and utilizing relevant resilience indicators [10–28]. Accurately assessing the impacts of outages from natural disasters or disruptive events on energy customers remains challenging [10–28]. Failing to quantify these impacts using appropriate resilience metrics can hinder decision makers' ability to identify optimal infrastructure investments [12–15,18–24]. While existing research has made contributions, limitations remain. Studies often lack diverse case studies, neglecting various weather conditions and their impact on system behavior [10–20]. Standardized resilience metrics specific to natural disasters are lacking, making it challenging to quantify the effectiveness of resilience-enhancing strategies [14–19]. Accurately measuring the impact of outages on consumers across diverse weather conditions remains challenging. Furthermore, previous research often overlooked the potential of BEVs, hybrid renewable energy sources, and effective microgrid formation [10–19].

This study aimed to address these challenges by analyzing and evaluating potential enhancements in power distribution system resilience against natural disasters using suitable metrics. The resilience analysis focused on two case studies: moderate and severe damage, considering various weather conditions, such as clear, cloudy, rainy, and sunny days. Through these analyses, this study sought to develop a comprehensive understanding of the role of DERs and BEVs in enhancing power grid resilience and inform decision-

making processes for infrastructure improvements. Specifically, it evaluated outage impacts on system loads in the IEEE 69-bus RDS using a networked EMG mechanism, integrating DERs, like SPV panels, WTs, BESSs, and BEVs, to form autonomous microgrids. The optimal allocation of DERs and BEVs were determined by a novel optimization algorithm called the slime mold algorithm (SMA) in the RDS. Additionally, it assessed the impacts on utility operators and customers due to natural disasters using new resilience indices. By contributing to the state-of-the-art in power distribution grid resilience, this study enhanced the system's capabilities under various natural disaster scenarios. This study introduced several novel contributions and methodologies aimed at enhancing the resilience of RDSs:

- The application of a novel optimization algorithm, namely, SMA, for sizing and siting DER and BEV components comprehensively addresses resilience challenges.
- The integration of DERs and BEVs into the RDS, forming autonomous microgrids, offers innovative solutions for bolstering system resilience during disruptions.
- The introduction of new resilience indices facilitates the measurement and analysis of system resilience under various scenarios, including different weather conditions and severity levels of damage.
- The assessment of the impact of natural disasters on utility operators and customers using these new resilience indices provides valuable insights for identifying mitigation strategies and improving system resilience.
- The utilization of the SMA-based system effectively manages DER sources to maximize economic and environmental benefits of the RDS.
- Investigation into the impact of contingency occurrences in EMGs enhances the management process and overall resilience.
- The development of detailed resilience metrics analysis that incorporates technical and economic parameters highlights the potential benefits of effectively managing DERs in prosumer-centric networked MGs.

The framework of this study focused on introducing innovative methods to enhance the resilience of electric power distribution systems, particularly in the face of natural disasters and disruptions. The significance of this framework lies in its capacity to effectively address challenges posed by such events. Through a comprehensive approach, this study aimed to enhance resilience during natural hazards by optimally utilizing DERs and BEVs within EMGs, which was facilitated by the SMA. Figure 1 provides a visual representation of this framework, illustrating the integration of DERs and BEVs into EMGs to improve resilience. By outlining these proposed methods and their significance, the framework provides a roadmap for addressing critical issues and improving the resilience of electric power distribution systems.

The following sections of this study are structured as follows: Section 3 describes the system modeling for resilience metric calculations and introduces the proposed optimization algorithm devised for addressing the resilience problem in the EMG. Section 4 presents the case study and numerical results, which were conducted using the standard IEEE 69-bus RDS. Finally, Section 5 provides a summary of the main conclusions drawn from this study.

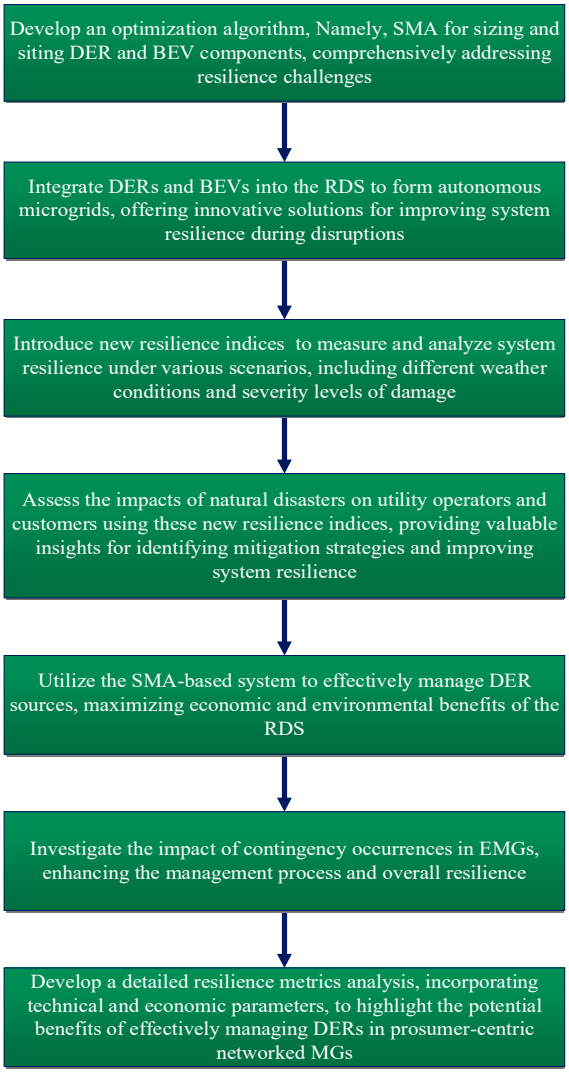


**Figure 1.** Visual representation of the proposed approach.

## 3. System Modeling for Resilience Metric Calculations

This section emphasizes the problem formulation, entailing the specification of objective functions, system limitations, and resilience indices. The primary objective was to enhance resilience indices while reducing operational expenses and improving critical load restoration. This necessitated the adherence to operational limits and ensuring radial operation within the distribution grid, which encompassed EMG and DERs. The resilience analysis process was employed to assess the resilience of this grid arrangement.

Figure 2 shows the sample households (prosumers) in a distribution system with the proposed approach. In the diagram, $V_m$ indicates the bus voltage at bus m, while $R_m$ and $X_m$ represent the resistance and reactance between the buses, respectively. Similarly, $P_m$ and $Q_m$ denote the real and reactive power flows between the buses in the RDS. Additionally, $P_{BESS}$, $P_{SPV/WT}$, and $P_{BEV}$ represent the power supplied by the BESS, SPV/WT, and BEV to the EMG.

The suggested approach intends to improve the distribution system resilience by creating prosumer-centric networked electrical microgrids that leverage DERs. These microgrids are intended to serve individual households, converting them into active players known as "prosumers" in the energy ecosystem. Integrating multiple DERs into the EMGs is a critical component of this system, including rooftop solar PV panels that generate electricity locally from solar energy and strategically located wind turbines that catch and convert wind energy into renewable power. These families can increase their

energy self-sufficiency and lessen their reliance on the centralized grid by combining solar and wind energy. BESSs are integrated into microgrids to improve the system resilience even more. These storage devices are critical for storing excess renewable energy during times of low demand or high output. When peak demand or RESs are unavailable, the stored energy can be used to ensure a consistent and reliable energy supply. This novel strategy aims to empower households, increasing their self-sufficiency and contributing to a stronger and sustainable RDS.

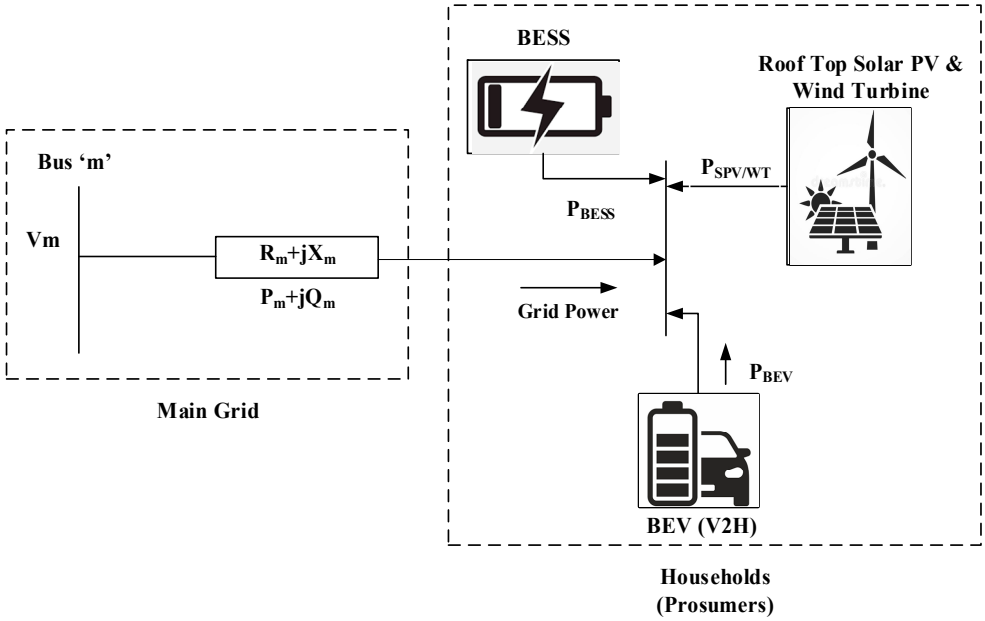


**Figure 2.** Sample households (prosumers) in distribution system with proposed approach.

The suggested method integrates BEVs into the distributed energy network as mobile energy storage units. This connection enables the surplus power generated during periods of surplus to be used to charge BEVs, improving the overall energy storage capacity. During periods of high demand or emergencies, these charged vehicles can feed energy back into the grid or power critical appliances, and thus, increase the RDS's resilience. The prosumer-centric approach enables homes to actively participate in the energy market, becoming not just customers but also generators, distributors, and storage facilities. Decentralized microgrids improve the system resilience by operating autonomously during grid outages or natural disasters, providing a localized power supply. Furthermore, the interconnected network of prosumer-centric microgrids allows for surplus energy to be shared between neighboring houses, fostering community resilience and contributing to a more sustainable and ecologically friendly energy landscape.

### *3.1. Resilience Metrics Formulation*

The significance and resilience metrics were classified into two categories:

(i) Resilience metrics for electrical utility;
(ii) Resilience metrics for cost analysis.

Each measure was calculated in the following manner.

#### 3.1.1. Formulation of Resilience Metrics for Electrical Utility ($\alpha$)

(a) Number of hours of outage for total households ($\alpha_1$):

$$\alpha_1 = \sum_{j=1}^{b} HH_j * t \quad (1)$$

where $(HH_j * t)$ in (1) is the number of hours spent by households during the outage and 'b' is the total number of buses in the RDS.

(b) Energy not supplied to all households ($\alpha_2$):

$$\alpha_2 = \sum_{j=1}^{b} ENS_j * t \tag{2}$$

where $(ENS_j * t)$ in (2) is the amount of household energy not supplied (ENS) during the outage.

(c) Total no. of households affected during the outage ($\alpha_3$):

$$\alpha_3 = \sum_{c=1}^{T_c} \sum_{j=1}^{b} HH_{j,c} \tag{3}$$

where $\alpha_3$ in (3) is the total number of households affected by the case 'c' outage and '$T_c$' is the total number of instances.

(d) Average number of households impacted ($\alpha_4$):

$$\alpha_4 = \frac{\sum_{c=1}^{T_c} \sum_{j=1}^{b} HH_{j,c}}{T_c} \tag{4}$$

In the provided Equation (4), $\alpha_4$ represents the average number of households affected during the outage in case 'c'.

3.1.2. Formulation of Resilience Metrics for Cost Analysis ($\beta$)

(a) Total revenue loss for utilities ($\beta_1$):

$$\beta_1 = C_e * \left( \sum_{j=1}^{b} ENS_j * t \right) \tag{5}$$

$$\beta_1 = C_e * \alpha_2 \tag{6}$$

In Equation (5), $\beta_1$ represents the total revenue loss from utilities (USD), and $C_e$ in (6) denotes the cost of energy (USD/kWh).

(b) Total costs incurred during the outage $(\beta_2)$:

$$\beta_2 = C_{out} * \left( \sum_{c=1}^{T_c} \sum_{j=1}^{b} HH_{j,c} \right) \tag{7}$$

$$\beta_2 = C_{out} * \alpha_3 \tag{8}$$

where $\beta_2$ in (7) is the total outage cost (USD) and $C_{out}$ in (8) is the outage cost per hour (USD/h).

(c) Total costs avoided during the outage $(\beta_3)$:

$$\beta_3 = C_{out,base} - \beta_2 \tag{9}$$

where $\beta_3$ is the avoided cost (USD) and $C_{out,base}$ is the total outage cost (USD) of the base case in (9).

(d) Proposed resilience index (RI):

Estimating a system's resilience index (RI) in the event of a catastrophic event entails computing the reciprocal of the system's loss performance, as specified in Equation (10).

$$RI = \frac{1}{\Delta P_L} \tag{10}$$

In the preceding Equation (10), $\Delta P_L$ represents the amount of generated real power that is inaccessible to the test system. As a result, Equation (11) can be used to calculate $\Delta P_L$:

$$\Delta P_L = \frac{P_{TL} - P_{AL}}{P_{AL}} \tag{11}$$

where $P_{TL}$ and $P_{AL}$ are the total load and active load in the system after the event occurs, respectively.

As a result, the level of resilience can be quantified on a theoretical scale ranging from 0 to infinity. Perfect resilience is expressed as infinity, signifying that no performance deterioration happens following an extreme event, whereas the absence of resilience is denoted by 0, implying a disaster to survive or an immediate collapse following the severe event.

### *3.2. Mathematical Formulation of Proposed Objective Function*

The aim of this study was to evaluate the efficiency of an RDS in terms of its resilience to natural disasters. The proposed methodology highlights a crucial goal of maximizing the overall power restoration for loads, as illustrated in Equation (12). The strategy prioritizes load recovery depending on their priority levels, ensuring a systematic recovery process in the event of natural disasters.

$$\text{Objective Function (F)} = \text{Maximize}\left(\sum_{c=1}^{T_c}\left(\frac{1}{\Delta P_{L,c}}\right)\right) \tag{12}$$

Equations (1)–(12) in this study were adopted from references [27,29] and were modified based on the specific requirements of our research. Meanwhile, Equations (13)–(18), which were utilized in the algorithms, were sourced from the original SMA article [30] and were adapted to accommodate the allocation of DERs and BEVs in an RDS.

### *3.3. Proposed SMA Optimization Algorithm*

The optimal allocation of DERs and BEVs within an EMG is crucial for enhancing resilience. By strategically placing DER and BEV assets based on demand patterns, renewable energy availability, and grid constraints, the microgrid can better withstand and recover from disruptions, such as grid outages or extreme weather events. DERs, including solar panels and wind turbines, coupled with BESSs, can provide localized power generation and storage capabilities, reducing the dependence on centralized grids. Meanwhile, BEVs can serve as mobile energy storage units, offering additional flexibility in balancing supply and demand within the microgrid. Through optimal allocation, the EMG can improve the energy reliability, minimize the downtime, and enhance the overall resilience to external disturbances, ultimately ensuring continuous and reliable power supply to critical loads.

#### 3.3.1. Overview

The proposed approach utilizes the recently developed nature-inspired SMA introduced by Li, Shimin et al. [30,31]; it draws inspiration from the natural behavior of slime mold. This algorithm mathematically depicts slime mold behavior through three primary stages, namely, food attraction, food enclosure, and oscillatory movements, enabling it to efficiently optimize the allocation of DER and BEV resources within EMGs.

#### 3.3.2. Approach Food

In the approach to food, slime mold behavior is guided by the scent in the surrounding air, enabling it to navigate toward food sources. This behavior is mathematically described by Equation (13):

$$S(t+1) = \begin{Bmatrix} S_i(t) + \partial_2 * (w_a * S_I(t) - S_J(t)), \partial_1 < p_{index} \\ \partial_3 * S(t), \partial_1 \geq p_{index} \end{Bmatrix} \tag{13}$$

In this equation, S represents the slime mold's position, and $S_j$ represents the current place with the strongest odor (indicating the presence of food). Individuals $S_I$ and $S_J$ were chosen at random from the slime mold community. The variable t represents the current iteration, while the value $\partial_1$ is uniformly generated between 0 and 1. The parameter $w_a$ represents the slime mold's adaptive weight, while $\partial_2$ is a value created evenly throughout the range [−x, x]. Furthermore, $\partial_3$ is a uniformly generated parameter within the range of [−y, y], where y gradually decreases from 1 to 0 based on the iteration ($y = 1 - t/Iter^{max}$). The probability index $p_{index}$ varies dynamically in response to Equation (14):

$$p_{index} = \tanh|S(i) - f_{best}| \tag{14}$$

In Equation (14), i represents the range of values from 1 to $n_{pop}$(the total population size), S(i) represents S's fitness value, and $f_{best}$ represents the best fitness obtained thus far. The parameter x is found using the provided Equation (15) to discover $\partial_2$:

$$x = \operatorname{arctanh}\left(-\left(\frac{t}{Iter^{max}}\right) + 1\right) \tag{15}$$

$$xw_a(Smell_{Index}(i)) = \left\{ \begin{array}{l} 1 + \partial_1 * \log\left(\frac{f_{optimal} - g(i)}{f_{favorable} - w_a F} + 1\right), \text{First half population} \\ 1 - \partial_1 * \log\left(\frac{f_{optimal} - g(i)}{f_{favorable} - w_a F} + 1\right), \text{Last half population} \end{array} \right\}, \tag{16}$$

$$xSmell_{Index} = \operatorname{sort}(g) \tag{17}$$

The present version uses the optimal fitness value ($f_{optimal}$) and the least favorable fitness value ($f_{favorable}$), as well as an ordered series of fitness values ($Smell_{Index}$).

3.3.3. Wrap Food

As it approaches the feeding phase, the SMA modifies its search mechanism to account for the concentration of food. The weight of an area reduces when the food concentration drops, but increasing the food concentration leads to a larger weight for the region. To improve the SMA's exploration phase, the slime mold's position can be updated using the equation below (18):

$$S^*(t+1) = \left\{ \begin{array}{c} v_{rand} * (u_l - l_l) + l_b, \partial_1 < c \\ S_j(t) + \partial_2 * (w_a * S_i(t) - S_J(t)), \partial_1 < p_{index} \\ \partial_3 * S(t), \partial_1 \geq p_{index} \end{array} \right\} \tag{18}$$

In the presented Equation (18), $u_l$ and $l_l$ denote the upper and lower bounds of the choice variables, respectively, while "rand" denotes a randomly generated number between 0 and 1. The value "c" was precisely allocated as 0.03 based on prior studies that found it to be the ideal value. The algorithm uses the maximum iteration, denoted as $Iter^{max}$. To simulate the formation of positive and negative feedback in the propagation wave of slime mold, an adaptive weight ($w_a$) is calculated using Equations (16) and (17) above.

3.3.4. Oscillation

In the equations above, the parameters $w_a$, $\partial_2$, and $\partial_3$ are used to capture the dynamics of slime mold during its food-finding activity. These parameters are used to simulate the changes in slime mold behavior as it hunts for the best food source. The oscillation frequency, represented by $w_a$, is mathematically incorporated to improve the slime mold's effectiveness in determining the most suitable food source. This frequency controls how fast the slime mold approaches a high-concentration food region and how slowly it approaches a low-concentration food area. As seen in Equation (18), the variable $\partial_2$ oscillates randomly throughout the range [−x, x] and progressively converges to zero with increasing iterations. Similarly, the variable $\partial_3$ exhibits stochastic oscillations in the range [−1, 1] and progressively converges to zero as the number of iterations increases. These characteristics are

inspired by the behavior of slime mold, which actively explores new territory in a quest for more food supplies while avoiding being trapped in local optima. The flowchart in Figure 3 depicts the process used by the SMA to handle difficulties and create appropriate solutions.

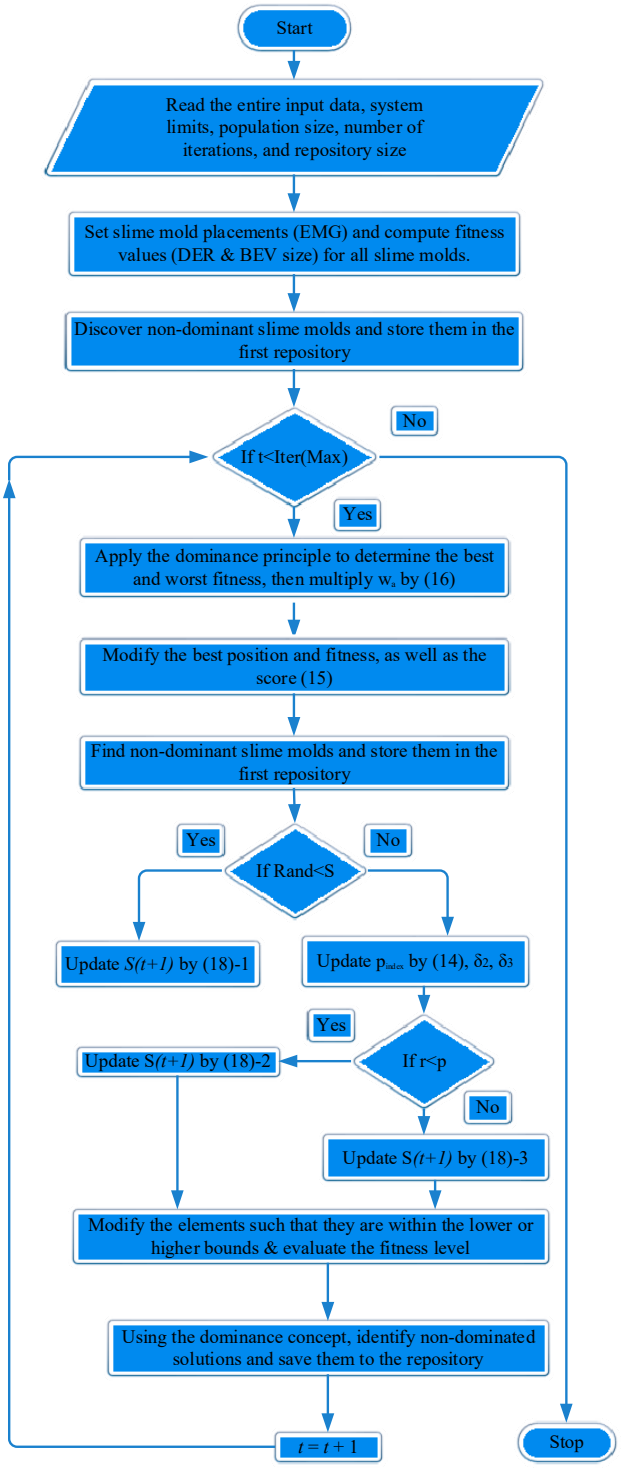


**Figure 3.** Slime mold algorithm flow chart for proposed approach.

## 4. Case Study and Numerical Results

The resilience measures outlined in the preceding subsections are examined in this section through two case studies conducted under distinct weather conditions: study I (moderate damage) and study II (severe damage). Residential customers with roof-top solar

PV, wind turbines, BEVs, and BESSs were assumed in the case studies. A customized 69-bus test system with four EMGs was used to run the simulations. Each case was compared with a base case that did not include DERs. It should be noted that the DERs were supposed to continue, even after a major event. The simulations spanned 24 h, including a four-hour period following a natural disaster when outages occurred. The ENS costs were estimated using a fixed energy rate of 0.16 USD/kWh [32]. Furthermore, the outage costs were calculated at a rate of 5.1 USD/h [33]. A severely damaged system was one in which more than 70% of the loads were still unserviced as a result of severe effects on RDS poles and lines. It was otherwise classified as a moderate disaster.

The predicted 4 h duration for the line restoration was based on an analysis of power outages in the USA caused by numerous big and minor occurrences [34]. To allow for a fair comparison of different cases, all lines were considered to be repaired concurrently and within the same timeframe. The case studies centered on a 69-bus RDS with 904 households spread across four EMGs. The original IEEE 69 test system is depicted in Figure 4 [35]. The results reported in this study were simulated and conducted using MATLAB R2019a on a personal computer with a 2.8 GHz CPU and 8 GB of RAM.

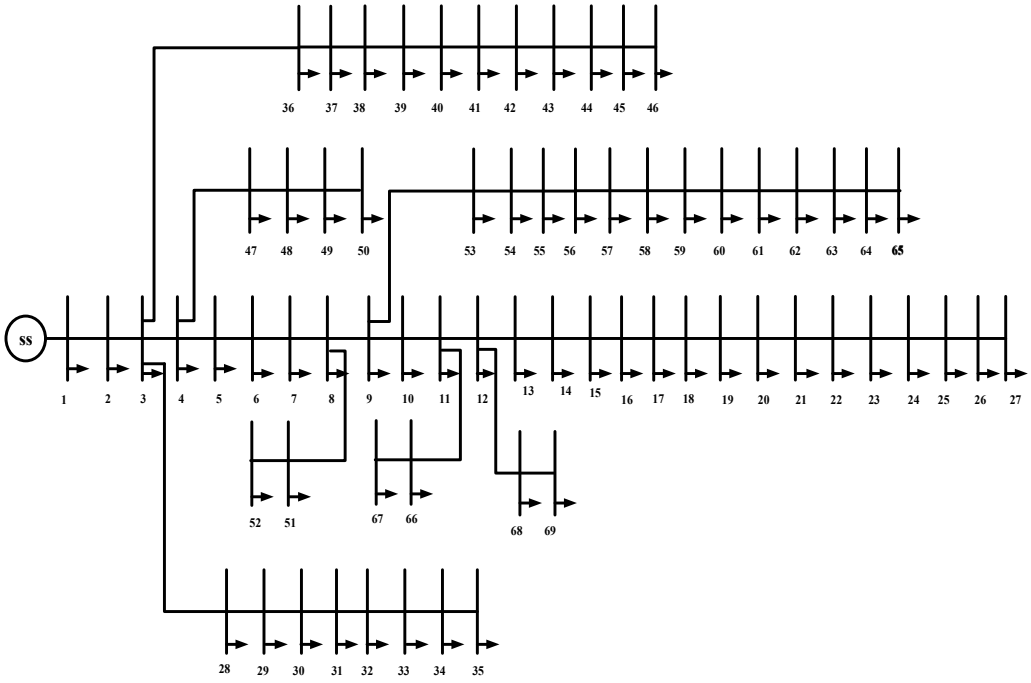


**Figure 4.** IEEE 69-bus RDS.

Several newly announced BEV models on the market have excellent driving ranges of more than 200 miles and battery capacities ranging from 60 kWh to 100 kWh [36]. Interestingly, 5 of the top 10 best-selling EVs in the USA have battery sizes of 60 kWh or above, indicating a notable industry trend. As a result, future EV models will almost certainly embrace bigger battery sizes as the new standard in most RDSs. This study chose the Tesla Model S [37] for the purposes of this EV modeling investigation. The Model S series includes a variety of battery capacity options, with our simulations focusing on the 70 kWh battery model. Based on a 240 V and 40 A connection, we assumed a maximum charging power of 10 kW. As a result, the simulations established the EV's minimum and maximum states of charge (SOCs) at 20% and 100%, respectively. The BESS in the simulations was a Tesla Powerwall [38]. The Powerwall's battery capacity is 13.5 kWh, with a charging/discharging power rating of 4 kW. The SOCs of the BESS are fixed at 0% and 100%, respectively. All information and parameter values for the BEV and BESS modeling were sourced from reference [39]. For the case studies, the following assumptions were made:

- It was presupposed that consumers/prosumers possessed a home energy management system.
- Each prosumer was outfitted with roof-top solar and wind turbines, as well as a BESS and BEV in the EMG.
- The examination of BEV charging was restricted to the consumer/prosumer household level, with no charging allowed between 6 a.m. and 6 p.m.
- Maintaining the BEV's SOC at or above 20% was imperative throughout the day.
- Line repairs were expected to take four hours and were scheduled from 10 a.m. to 2 p.m.
- All power lines underwent simultaneous repairs, ensuring each line received equal attention.
- During a power outage, all vital loads were presumed to be situated within the EMGs and were served first.
- To maintain consistency in the comparisons, fault locations and EMG formations remained identical across all cases.
- The BEV ran in vehicle-to-home (V2H) mode, allowing for power to be transferred from the home to the grid.
- The power outputs of the solar PV/wind turbines, BEVs, and BESSs under different weather conditions, as extracted from Tables 2–6 of references [33,39], were adapted for use in the proposed study.

Figure 5 depicts the power demand statistics for the IEEE 69-bus system for each bus. Figures 6 and 7 show the output powers of solar PV and wind turbines under various weather situations (clear, cloudy, rainy, and sunny days), which were taken into account for the case studies. These profiles were expected to be uniform for all residential classified prosumers. Each prosumer's solar PV and wind turbine installations were sized at 5 kW and 6 kW, respectively, to meet two times their peak demand. This sizing assured that the roof-top solar PV array and windmills could meet the demand of prosumers in most weather circumstances, including low solar irradiation. The BESS size for each prosumer was determined by the projected excess energy production. The optimal allocation of these device sizes within the EMGs could be achieved using the SMA optimization technique. Table 1 shows the output power values of solar PV and wind turbines for the various weather situations evaluated in the case studies.

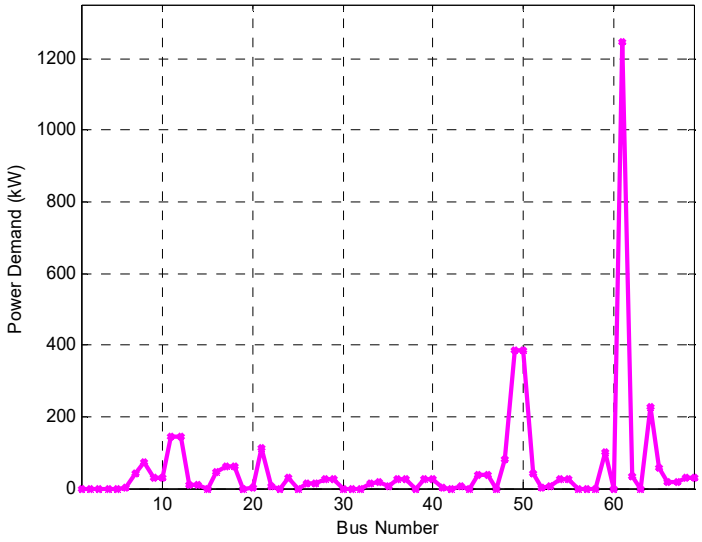


**Figure 5.** Power demand of IEEE 69-bus system.

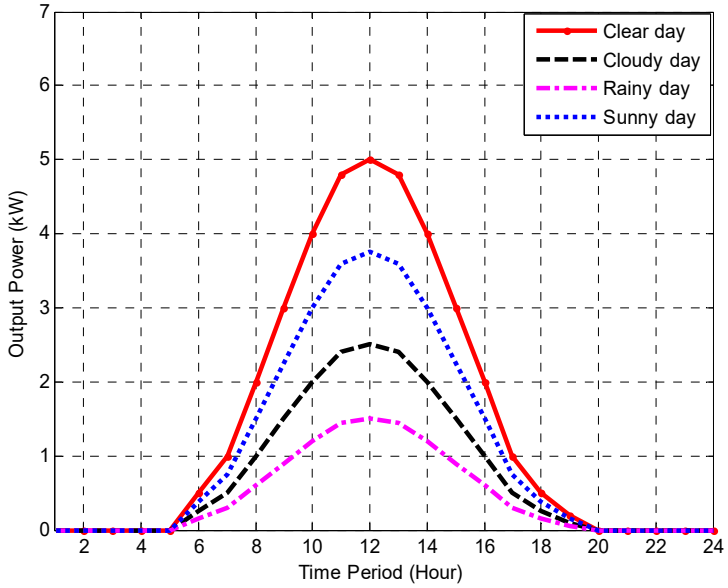


**Figure 6.** Solar PV output power during various weather conditions.

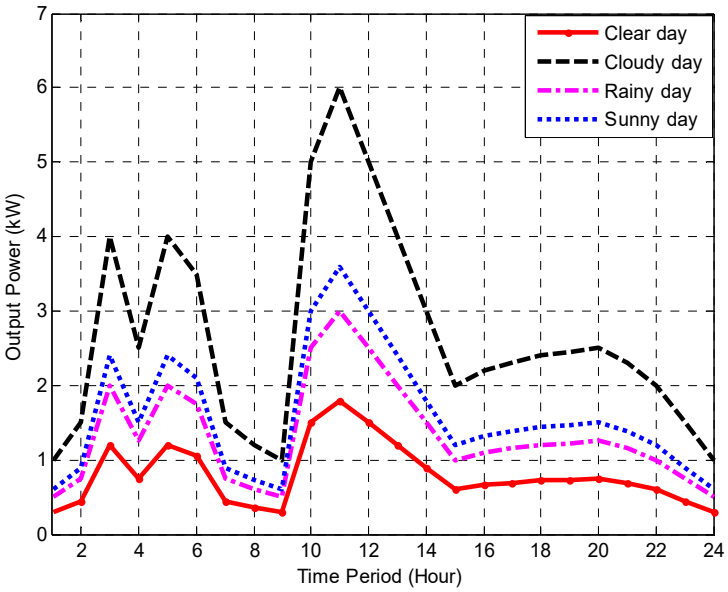


**Figure 7.** Wind turbine output power during various weather conditions.

**Table 1.** Solar PV/wind turbine output powers under various weather conditions.

| Session/Weather | Solar PV Power Output (%) | Wind Turbine Power Output (%) |
|---|---|---|
| Clear day | 100% | 30% |
| Cloudy day | 50% | 100% |
| Rainy day | 30% | 50% |
| Sunny day | 75% | 60% |

The following four different cases were considered for the moderate damage study.

### *4.1. Study I (Moderate Damage)*

#### 4.1.1. Without Any DERs

In the base case, the RDS was not connected to any DERs. The IEEE 69-bus test system operated on a typical grid, but it confronted difficulties during the day, particularly at

10 a.m., when four independent faults occurred. These failures caused a 4 h outage that affected certain buses, including buses 16–22, 28–35, 39–46, and 60–65 (Figure 8). As a result, a large amount of the load, around 2073 kW of the total 3801 kW load, suffered during this period. When the base case performance was examined, troubling findings emerged. Notably, the ENS value reached 8292 kWh, indicating a significant energy deficit during the outage. Moreover, the RI value was limited to 0.76, which was primarily attributed to the absence of a backup unit in the system. Consequently, during fault occurrences, the entire load was disconnected from the grid power, posing potential interruptions and reliability concerns.

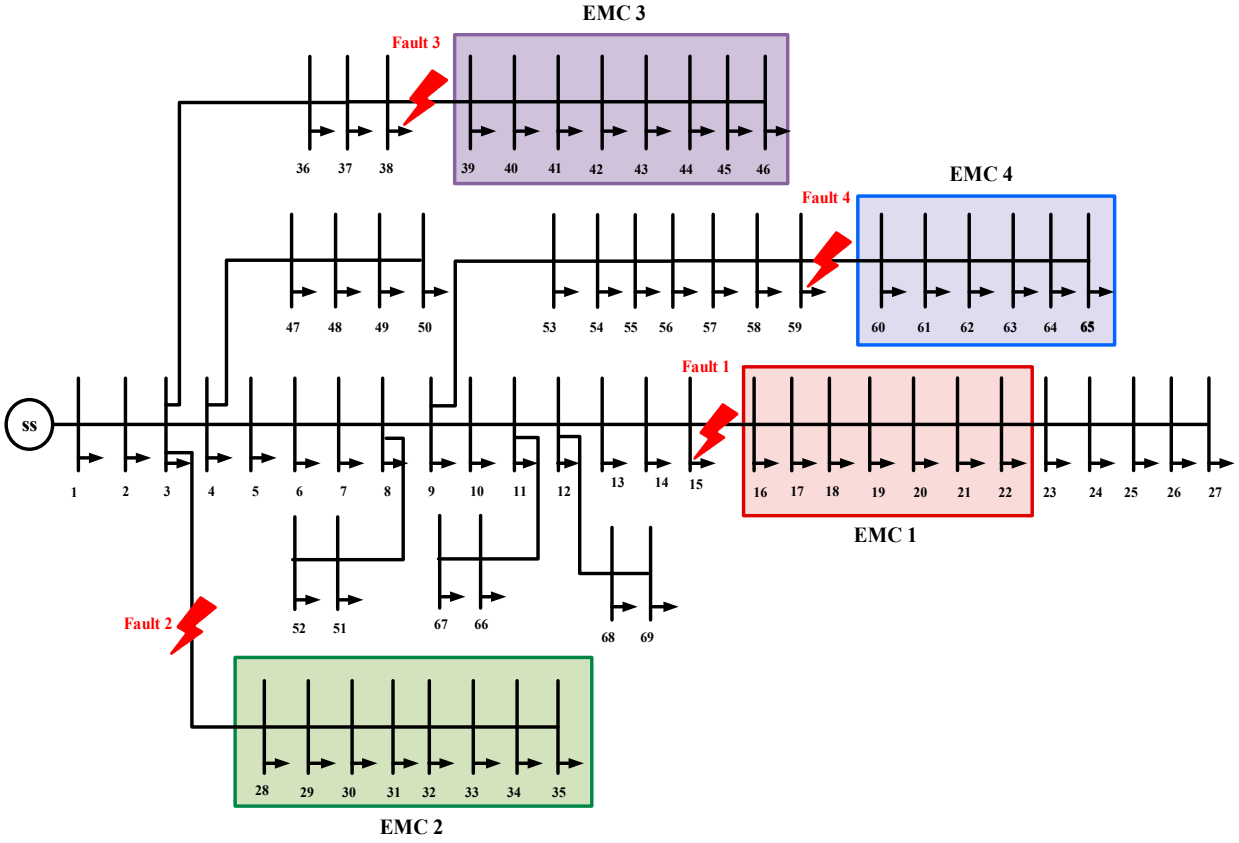


**Figure 8.** IEEE 69-bus RDS without any DERs (study I).

The introduction of DERs into the RDS has the potential to increase its reliability and performance under adverse conditions while also enhancing sustainability and efficiency. Moreover, DERs, especially energy storage devices, assume a pivotal role by storing surplus energy during periods of low demand or high RES. This stored energy serves to ensure a consistent power supply and reduce the size of the ENS during faults or outages, particularly at peak demand. Additionally, DERs contribute auxiliary services, such as frequency regulation and voltage support, thereby assisting in the preservation of grid stability. The integration of DERs into the RDS holds the promise of elevating its reliability and performance under adverse conditions, concurrently bolstering the sustainability and efficiency.

#### 4.1.2. Clear Day with DERs

The current resilience challenge assumed clear weather conditions and sought to address a variety of operating tactics, including varied weather scenarios. Weather has a significant impact on energy generation from rooftop solar and wind generators, as well as the BESS's energy storage capacity for dispatch during crucial events. Table 2 demonstrates the typical power output levels of all the resources under consideration. Table 3 presents simulation statistics for a solar PV (100%) and wind turbine (30%) on clear days, based on

their usual power output levels. Table 2 demonstrates the typical power output levels of all the resources under consideration. Table 3 presents simulation statistics for a solar PV (100%) and wind turbine (30%) on clear days, based on their usual power output levels. The maximum power outputs for the solar PV and wind turbine were 725 kW and 252 kW, respectively, as shown in the table. Furthermore, the aggregate power capacities of the BEV and BESS were 650 kW and 535 kW, respectively, and were consistent across all situations. When the solar PV and wind turbine electricity were absent, the BESS units released stored energy to power the EMGs.

The presence of four EMGs, each depicted by a dotted line in Figure 8, was taken into account in an IEEE 69-bus RDS. The RDS in question comprised DERs and BEVs operating in V2G mode. During power outages, BEVs can serve as mobile energy storage devices, supplying power back to the grid. The deployment of DERs on buses across all EMGs was anticipated to decrease the necessity for load curtailment in various scenarios. The system aimed to recover some of the lost power during outages by integrating DERs in the EMGs, as illustrated in Figure 9, where DERs were added to all IEEE 69-bus EMGs. Furthermore, the RI improved to 4.42, while the ENS decreased to 2804 kWh. This indicates that allocating DERs to the EMGs enhanced the overall system resilience.

**Table 2.** Simulation data for IEEE 69-bus RDS.

| EMG | Prosumer (P)/Consumer (C) | Bus | Households | Load (kW) | Solar PV (kW) | Wind Turbine (kW) | BEV (kW) | BESS | |
|---|---|---|---|---|---|---|---|---|---|
| | | | | | | | | Capacity (kWh) | Output (kW) |
| EMG 1 | P | 16 | 12 | 46 | 60 | 72 | 40 | 324 | 60 |
| | P | 17 | 16 | 60 | 80 | 96 | 50 | 432 | 80 |
| | C | 18 | 16 | 60 | - | - | 0 | - | - |
| | C | 19 | 0 | 0 | - | - | 0 | - | - |
| | C | 20 | 0 | 1 | - | - | 0 | - | - |
| | C | 21 | 28 | 114 | - | - | 0 | - | - |
| | P | 22 | 2 | 5 | 10 | 12 | 30 | 108 | 20 |
| EMG 2 | C | 28 | 6 | 26 | - | - | 0 | - | - |
| | P | 29 | 6 | 26 | 30 | 36 | 50 | 162 | 30 |
| | C | 30 | 0 | 0 | - | - | 0 | - | - |
| | C | 31 | 0 | 0 | - | - | 0 | - | - |
| | C | 32 | 0 | 0 | - | - | 0 | - | - |
| | P | 33 | 4 | 14 | 20 | 24 | 30 | 108 | 20 |
| | C | 34 | 5 | 19.5 | - | - | 30 | 108 | 20 |
| | P | 35 | 2 | 6 | 10 | 12 | 30 | 54 | 10 |
| EMG 3 | P | 39 | 6 | 24 | 30 | 36 | 50 | 162 | 30 |
| | P | 40 | 6 | 24 | 30 | 36 | 50 | 162 | 30 |
| | C | 41 | 0 | 1.2 | - | - | 0 | - | - |
| | C | 42 | 0 | 0 | - | - | 0 | - | - |
| | P | 43 | 2 | 6 | 10 | 12 | 30 | 108 | 20 |
| | C | 44 | 0 | 0 | - | - | 0 | - | - |
| | P | 45 | 10 | 39.22 | 50 | 60 | 60 | 270 | 50 |
| | C | 46 | 10 | 39.22 | - | - | 0 | - | - |
| EMG 4 | C | 60 | 0 | 0 | - | - | 0 | - | - |
| | C | 61 | 700 | 1244 | - | - | 0 | - | - |
| | P | 62 | 8 | 32 | 40 | 48 | 70 | 216 | 40 |
| | C | 63 | 0 | 0 | - | - | 0 | - | - |
| | P | 64 | 50 | 227 | 250 | 300 | 70 | 270 | 50 |
| | P | 65 | 15 | 59 | 75 | 90 | 60 | 405 | 75 |

**Table 3.** Simulation data for IEEE 69-bus RDS (clear day).

| EMG | Prosumer (P)/Consumer (C) | Bus | Households | Load (kW) | Solar PV (kW) | Wind Turbine (kW) | BEV (kW) | BESS | |
|---|---|---|---|---|---|---|---|---|---|
| | | | | | | | | Capacity (kWh) | Output (kW) |
| EMG 1 | P | 16 | 12 | 46 | 60 | 22 | 40 | 324 | 60 |
| | P | 17 | 16 | 60 | 80 | 29 | 50 | 432 | 80 |
| | C | 18 | 16 | 60 | - | - | 0 | - | - |
| | C | 19 | 0 | 0 | - | - | 0 | - | - |
| | C | 20 | 0 | 1 | - | - | 0 | - | - |
| | C | 21 | 28 | 114 | - | - | 0 | - | - |
| | P | 22 | 2 | 5 | 10 | 4 | 30 | 108 | 20 |
| EMG 2 | C | 28 | 6 | 26 | - | - | 0 | - | - |
| | P | 29 | 6 | 26 | 30 | 11 | 50 | 162 | 30 |
| | C | 30 | 0 | 0 | - | - | 0 | - | - |
| | C | 31 | 0 | 0 | - | - | 0 | - | - |
| | C | 32 | 0 | 0 | - | - | 0 | - | - |
| | P | 33 | 4 | 14 | 20 | 7 | 30 | 108 | 20 |
| | C | 34 | 5 | 19.5 | - | - | 30 | 108 | 20 |
| | P | 35 | 2 | 6 | 10 | 4 | 30 | 54 | 10 |
| EMG 3 | P | 39 | 6 | 24 | 30 | 11 | 50 | 162 | 30 |
| | P | 40 | 6 | 24 | 30 | 11 | 50 | 162 | 30 |
| | C | 41 | 0 | 1.2 | - | - | 0 | - | - |
| | C | 42 | 0 | 0 | - | - | 0 | - | - |
| | P | 43 | 2 | 6 | 10 | 4 | 30 | 108 | 20 |
| | C | 44 | 0 | 0 | - | - | 0 | - | - |
| | P | 45 | 10 | 39.22 | 50 | 18 | 60 | 270 | 50 |
| | C | 46 | 10 | 39.22 | - | - | 0 | - | - |
| EMG 4 | C | 60 | 0 | 0 | - | - | 0 | - | - |
| | C | 61 | 700 | 1244 | - | - | 0 | - | - |
| | P | 62 | 8 | 32 | 40 | 14 | 70 | 216 | 40 |
| | C | 63 | 0 | 0 | - | - | 0 | - | - |
| | P | 64 | 50 | 227 | 250 | 90 | 70 | 270 | 50 |
| | P | 65 | 15 | 59 | 75 | 27 | 60 | 405 | 75 |

#### 4.1.3. Cloudy Day with DERs

The resilience improvement problem was addressed under the premise of cloudy weather circumstances, with solar generation at 50% and wind generation at 100%. The RDS took DERs into account as well. Table 4 shows the simulation data for the IEEE 69-bus RDS under these cloudy conditions. Notably, the maximum power output from the PV sources was substantially lower at 348 kW compared with the 695 kW in the clear day scenario. This equated to a 50% decrease in maximum solar PV power output. On the plus side, the maximum WT power production was 870 kW, which was 70% more than what was seen in the clear day simulations.

The restoration plan was initiated at 10 a.m. and spanned four hours until 2 p.m. The distribution of DERs within the EMG during this process led to a substantial reduction in the ENS value, decreasing from 8292 kWh (case 1) to 2306 kWh. Additionally, there was a notable decrease in the percentage of affected homes, with 173 houses (12.79%) impacted, compared with the typical rate of 43.25 (3.19%). The system's resilience indicators experienced a significant increase, elevating from 0.76 to 5.61.

#### 4.1.4. Rainy Day with DERs

Under wet conditions, the ideal location problem was handled. The PV and WT power figures for this case are shown in Table 5. Notably, the maximum SPV power achieved on a rainy day was 209 kW, which was 70% and 50% lower than the maximum SPV power achieved on clear (695 kW) and cloudy (348 kW) days, respectively. The highest power of

the WT system was 435 kW. This decrease suggests a significant improvement in the overall system performance, especially in terms of resilience. The RI achieved an astounding 3.38, demonstrating the system's improved ability to resist and recover from disturbances or prospective disruptions. This accomplishment was primarily due to the efficient allocation of DERs to EMGs. Another important indicator of system improvement is the lower ENS figure of 3474 kWh. A lower ENS number indicates that less energy demand went unmet during important events or poor conditions, highlighting the effectiveness of DERs in improving system dependability.

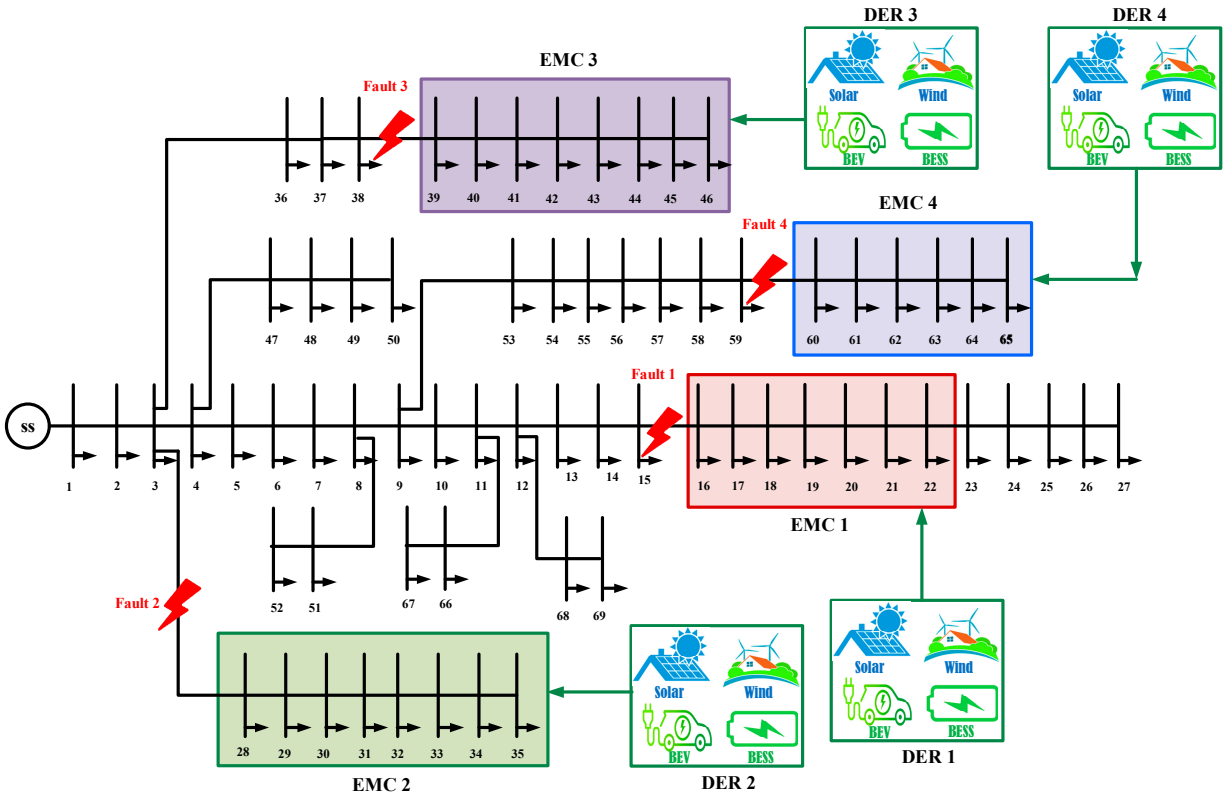


**Figure 9.** IEEE 69-bus RDS with DERs (study I).

A notable discovery on rainy days, the system's resilience values were significantly lower, but the ENS values were significantly greater than on clear and cloudy days. These findings imply that there is space to improve the system's effectiveness during bad weather by implementing focused improvements and specialized procedures. The installation of DERs, on the other hand, was shown to be highly effective in increasing the system's performance under different weather situations.

#### 4.1.5. Sunny Day with DERs

During sunny day conditions, the optimal location problem was addressed by considering PV and WT power. As indicated in Table 6, the maximum SPV power attained on a sunny day was 544 kW, which represented a 25% decrease compared with a clear day (695 kW). The highest power output from the WT system was 522 kW. Despite this decrease, there was a significant enhancement in the overall system performance, particularly in resilience aspects. The RI reached an impressive 3.38, indicating a notable improvement in the system's ability to withstand and recover from disturbances or potential disruptions. This achievement was primarily attributed to the effective allocation of DERs to EMGs. Another important measure of system enhancement was the reduced ENS value of 2642 kWh. A lower ENS value suggests that less energy demand remained unmet dur-

ing critical events or adverse conditions, underscoring the efficacy of DERs in enhancing system reliability.

**Table 4.** Simulation data for IEEE 69-bus RDS (cloudy day).

| EMG | Prosumer (P)/Consumer (C) | Bus | Households | Load (kW) | Solar PV (kW) | Wind Turbine (kW) | BEV (kW) | BESS | |
|---|---|---|---|---|---|---|---|---|---|
| | | | | | | | | Capacity (kWh) | Output (kW) |
| EMG 1 | P | 16 | 12 | 46 | 30 | 72 | 40 | 324 | 60 |
| | P | 17 | 16 | 60 | 40 | 96 | 50 | 432 | 80 |
| | C | 18 | 16 | 60 | - | - | 0 | - | - |
| | C | 19 | 0 | 0 | - | - | 0 | - | - |
| | C | 20 | 0 | 1 | - | - | 0 | - | - |
| | C | 21 | 28 | 114 | - | - | 0 | - | - |
| | P | 22 | 2 | 5 | 5 | 12 | 30 | 108 | 20 |
| EMG 2 | C | 28 | 6 | 26 | - | 36 | 0 | - | - |
| | P | 29 | 6 | 26 | 15 | 36 | 50 | 162 | 30 |
| | C | 30 | 0 | 0 | - | - | 0 | - | - |
| | C | 31 | 0 | 0 | - | - | 0 | - | - |
| | C | 32 | 0 | 0 | - | - | 0 | - | - |
| | P | 33 | 4 | 14 | 10 | 24 | 30 | 108 | 20 |
| | C | 34 | 5 | 19.5 | - | - | 30 | 108 | 20 |
| | P | 35 | 2 | 6 | 5 | 12 | 30 | 54 | 10 |
| EMG 3 | P | 39 | 6 | 24 | 15 | 36 | 50 | 162 | 30 |
| | P | 40 | 6 | 24 | 15 | 36 | 50 | 162 | 30 |
| | C | 41 | 0 | 1.2 | - | - | 0 | - | - |
| | C | 42 | 0 | 0 | - | - | 0 | - | - |
| | P | 43 | 2 | 6 | 5 | 12 | 30 | 108 | 20 |
| | C | 44 | 0 | 0 | - | - | 0 | - | - |
| | P | 45 | 10 | 39.22 | 25 | 60 | 60 | 270 | 50 |
| | C | 46 | 10 | 39.22 | - | - | 0 | - | - |
| EMG 4 | C | 60 | 0 | 0 | - | - | 0 | - | - |
| | C | 61 | 700 | 1244 | - | - | 0 | - | - |
| | P | 62 | 8 | 32 | 20 | 48 | 70 | 216 | 40 |
| | C | 63 | 0 | 0 | - | - | 0 | - | - |
| | P | 64 | 50 | 227 | 125 | 300 | 70 | 270 | 50 |
| | P | 65 | 15 | 59 | 37.5 | 90 | 60 | 405 | 75 |

The ENS profiles depicted in Figure 10a–e highlight the influence of different weather conditions and the integration of DERs on system resilience. Initially, without any DERs (case I), the ENS value peaked at 8292 kWh, indicating significant unmet energy demand during the outages. However, the integration of DERs on clear, cloudy, and rainy days (case II to case IV) consistently led to reduced ENS values, signaling enhanced system reliability and resilience. Notably, the lowest ENS value was observed on a cloudy day with DERs (case III) at 2306 kWh, followed closely by a sunny day with DERs (case II) at 2804 kWh, underscoring the effectiveness of DER integration, particularly under these weather conditions. This reduction in ENS values across these scenarios emphasized the importance of mitigating energy demand during disruptions to bolster system resilience. Specifically, case III stood out for providing the least ENS among all scenarios considered, highlighting its potential for significantly enhancing system resilience by minimizing the unmet energy demand during outages.

To compare the resilience metrics between different weather conditions, we could examine the outcomes presented in Tables 7 and 8 for case 1 to case 5 of the IEEE 69-bus system. In terms of the outage duration for total households, case 2 and case 3 showed the lowest values at 840 h and 692 h, respectively, indicating shorter periods of disruption compared with other cases. Similarly, in terms of ENS to all households, case 2 and case 3

also exhibited the lowest values of 2804 kWh and 2306 kWh, respectively, suggesting less of the energy demand went unmet during outages. Moreover, when considering the RI presented in Table 8, case 3 demonstrated the highest value at 5.61, followed closely by case 2, with a value of 4.42. However, case 5 also provided noteworthy results, with the outage duration and ENS values falling between case 3 and case 4, indicating relatively favorable resilience outcomes. Specifically, case 5 showed an outage duration of 792 h and an ENS value of 2642 kWh, along with a resilience index of 4.75. While case 5 did not surpass case 2 and case 3 in terms of resilience metrics, it still represented a significant improvement compared with case 1 and case 4. Overall, case 2, case 3, and case 5 showcased more favorable resilience outcomes compared with case 1 and case 4, with case 2 and case 3 performing slightly better across multiple metrics.

**Table 5.** Simulation data for IEEE 69-bus RDS (rainy day).

| EMG | Prosumer (P)/Consumer (C) | Bus | Households | Load (kW) | Solar PV (kW) | Wind Turbine (kW) | BEV (kW) | BESS | |
|---|---|---|---|---|---|---|---|---|---|
| | | | | | | | | Capacity (kWh) | Output (kW) |
| EMG 1 | P | 16 | 12 | 46 | 18 | 36 | 40 | 324 | 60 |
| | P | 17 | 16 | 60 | 24 | 48 | 50 | 432 | 80 |
| | C | 18 | 16 | 60 | - | - | 0 | - | - |
| | C | 19 | 0 | 0 | - | - | 0 | - | - |
| | C | 20 | 0 | 1 | - | - | 0 | - | - |
| | C | 21 | 28 | 114 | - | - | 0 | - | - |
| | P | 22 | 2 | 5 | 3 | 6 | 30 | 108 | 20 |
| EMG 2 | C | 28 | 6 | 26 | - | 18 | 0 | - | - |
| | P | 29 | 6 | 26 | 9 | 18 | 50 | 162 | 30 |
| | C | 30 | 0 | 0 | - | - | 0 | - | - |
| | C | 31 | 0 | 0 | - | - | 0 | - | - |
| | C | 32 | 0 | 0 | - | - | 0 | - | - |
| | P | 33 | 4 | 14 | 6 | 12 | 30 | 108 | 20 |
| | C | 34 | 5 | 19.5 | - | - | 30 | 108 | 20 |
| | P | 35 | 2 | 6 | 3 | 6 | 30 | 54 | 10 |
| EMG 3 | P | 39 | 6 | 24 | 9 | 18 | 50 | 162 | 30 |
| | P | 40 | 6 | 24 | 9 | 18 | 50 | 162 | 30 |
| | C | 41 | 0 | 1.2 | - | - | 0 | - | - |
| | C | 42 | 0 | 0 | - | - | 0 | - | - |
| | P | 43 | 2 | 6 | 3 | 6 | 30 | 108 | 20 |
| | C | 44 | 0 | 0 | - | - | 0 | - | - |
| | P | 45 | 10 | 39.22 | 15 | 30 | 60 | 270 | 50 |
| | C | 46 | 10 | 39.22 | - | - | 0 | - | - |
| EMG 4 | C | 60 | 0 | 0 | - | - | 0 | - | - |
| | C | 61 | 700 | 1244 | - | - | 0 | - | - |
| | P | 62 | 8 | 32 | 12 | 24 | 70 | 216 | 40 |
| | C | 63 | 0 | 0 | - | - | 0 | - | - |
| | P | 64 | 50 | 227 | 75 | 150 | 70 | 270 | 50 |
| | P | 65 | 15 | 59 | 22.5 | 45 | 60 | 405 | 75 |

Figures 11 and 12 provide a detailed comparison of the ENS values and RIs across different scenarios of the IEEE 69-bus system. Among these cases, case 3 stood out by exhibiting the lowest ENS value and the highest RI, indicating superior system resilience. This underscores the significant positive impact of strategically allocating DERs during cloudy days on the IEEE 69-bus RDS's resilience. The observed resilience gained in case 3 is promising and underscores the effectiveness of the DER allocation mechanism being studied. By optimizing the utilization of DERs during severe weather conditions, the system became better equipped to withstand and recover from disruptive events, ultimately enhancing its overall resilience. Furthermore, Figure 13 visually illustrates the entire averted

outage cost for the RDS before, during, and after the occurrence of disruptive events. Notably, case 3 emerged as the most advantageous option, demonstrating superior total averted outage cost compared with the other cases considered. This finding validates the efficacy of the proposed framework in enhancing the economic performance and reliability of the IEEE 69-bus RDS.

**Table 6.** Simulation data for IEEE 69-bus RDS (sunny day).

| EMG | Prosumer (P)/Consumer (C) | Bus | Households | Load (kW) | Solar PV (kW) | Wind Turbine (kW) | BEV (kW) | BESS | |
|---|---|---|---|---|---|---|---|---|---|
| | | | | | | | | Capacity (kWh) | Output (kW) |
| EMG 1 | P | 16 | 12 | 46 | 45 | 43 | 40 | 324 | 60 |
| | P | 17 | 16 | 60 | 60 | 58 | 50 | 432 | 80 |
| | C | 18 | 16 | 60 | - | - | 0 | - | - |
| | C | 19 | 0 | 0 | - | - | 0 | - | - |
| | C | 20 | 0 | 1 | - | - | 0 | - | - |
| | C | 21 | 28 | 114 | - | - | 0 | - | - |
| | P | 22 | 2 | 5 | 8 | 7 | 30 | 108 | 20 |
| EMG 2 | C | 28 | 6 | 26 | 23 | 22 | 0 | - | - |
| | P | 29 | 6 | 26 | 23 | 22 | 50 | 162 | 30 |
| | C | 30 | 0 | 0 | - | - | 0 | - | - |
| | C | 31 | 0 | 0 | - | - | 0 | - | - |
| | C | 32 | 0 | 0 | - | - | 0 | - | - |
| | P | 33 | 4 | 14 | 15 | 14 | 30 | 108 | 20 |
| | C | 34 | 5 | 19.5 | - | - | 30 | 108 | 20 |
| | P | 35 | 2 | 6 | 8 | 7 | 30 | 54 | 10 |
| EMG 3 | P | 39 | 6 | 24 | 22.5 | 21.6 | 50 | 162 | 30 |
| | P | 40 | 6 | 24 | 22.5 | 21.6 | 50 | 162 | 30 |
| | C | 41 | 0 | 1.2 | - | - | 0 | - | - |
| | C | 42 | 0 | 0 | - | - | 0 | - | - |
| | P | 43 | 2 | 6 | 7.5 | 7.2 | 30 | 108 | 20 |
| | C | 44 | 0 | 0 | - | - | 0 | - | - |
| | P | 45 | 10 | 39.22 | 37.5 | 36 | 60 | 270 | 50 |
| | C | 46 | 10 | 39.22 | - | - | 0 | - | - |
| EMG 4 | C | 60 | 0 | 0 | - | - | 0 | - | - |
| | C | 61 | 700 | 1244 | - | - | 0 | - | - |
| | P | 62 | 8 | 32 | 30 | 28.8 | 70 | 216 | 40 |
| | C | 63 | 0 | 0 | - | - | 0 | - | - |
| | P | 64 | 50 | 227 | 187.5 | 180 | 70 | 270 | 50 |
| | P | 65 | 15 | 59 | 56.25 | 54 | 60 | 405 | 75 |

**Table 7.** Resilience metrics for electrical utility (study I) of IEEE 69-bus system.

| Cases | Number of Hours of Outage for Total Households (h) | ENS to All Households (kWh) | Total Number and Percentage of Households Impacted | Average Number and Percentage of Households Impacted |
|---|---|---|---|---|
| Case 1 | 3616 | 8292 | 904 (66.86%) | 226 (16.71%) |
| Case 2 | 840 | 2804 | 210 (15.53%) | 52.5 (3.8%) |
| Case 3 | 692 | 2306 | 173 (12.79%) | 43.25 (3.19%) |
| Case 4 | 1044 | 3474 | 261 (19.30%) | 62.25 (4.82%) |
| Case 5 | 792 | 2642 | 198 (14.64%) | 49.5 (3.66%) |

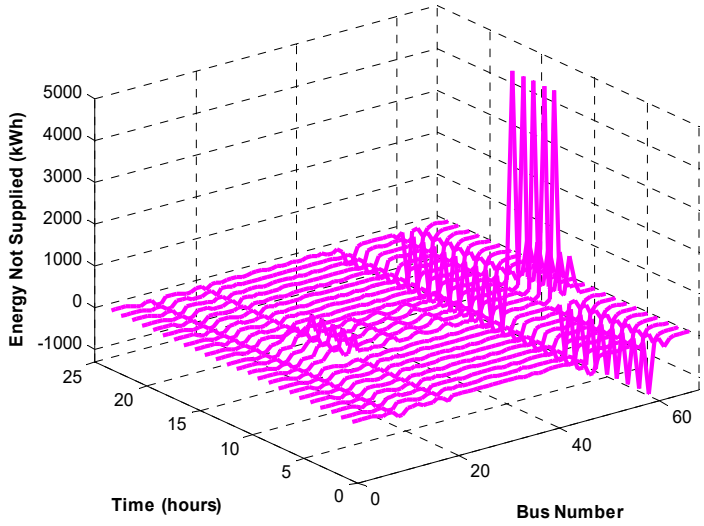


(**a**)

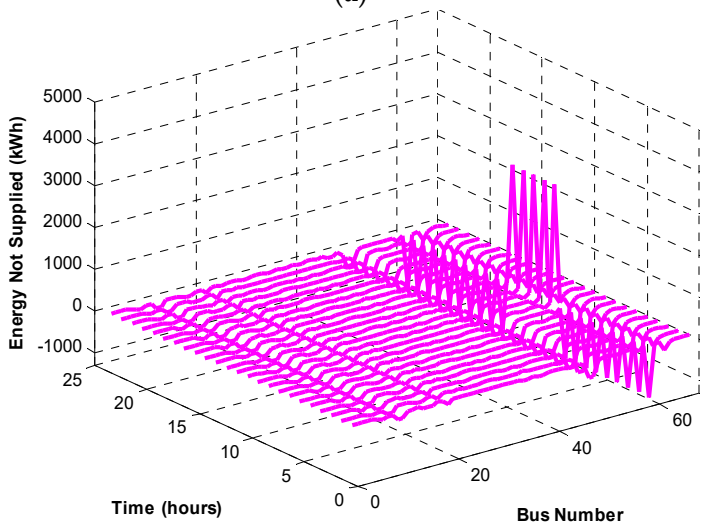


(**b**)

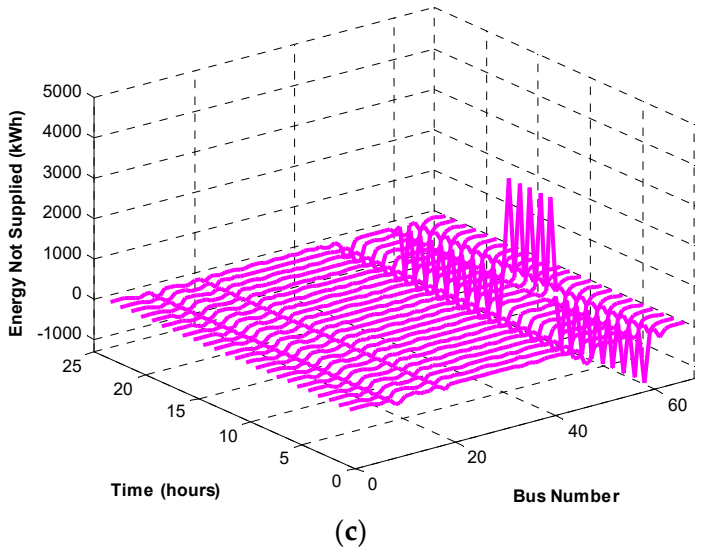


(**c**)

**Figure 10.** *Cont.*

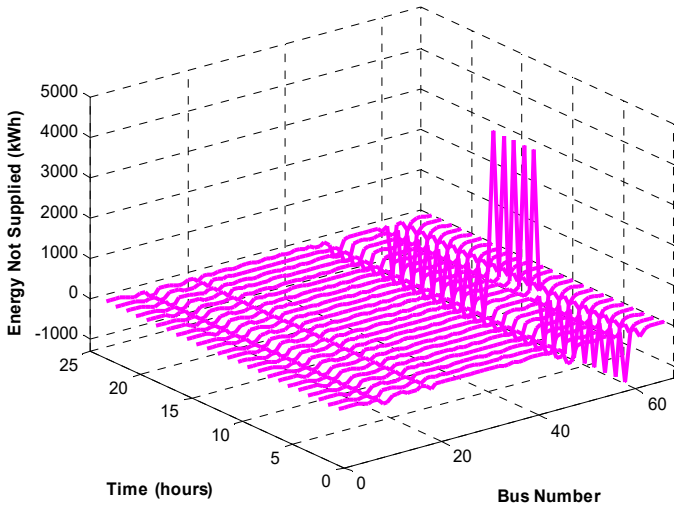


(**d**)

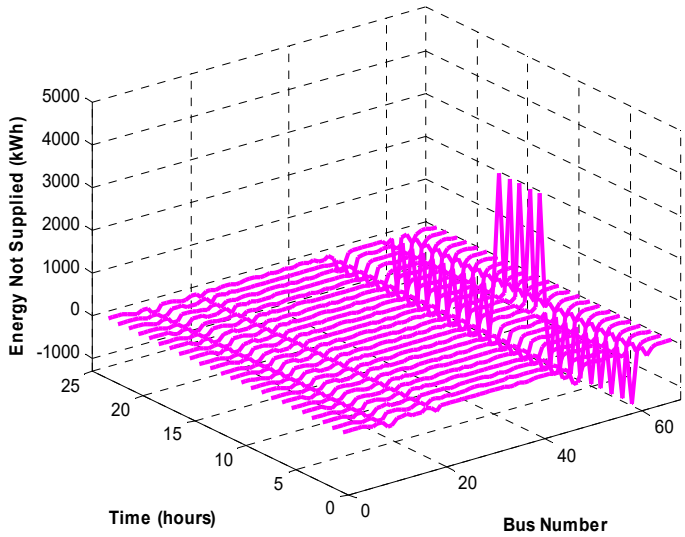


(**e**)

**Figure 10.** (**a**) ENS profile of case I (without any DERs, study I). (**b**) ENS profile of case II (clear day with DERs, study I). (**c**) ENS profile of case III (cloudy day with DERs, study I). (**d**) ENS profile of case IV (rainy day with DERs, study I). (**e**) ENS profile of case V (sunny day with DERs, study I).

**Table 8.** Resilience metrics for cost analysis (study I) of IEEE 69-bus system.

| Cases | Total Revenue Loss for Utilities (USD/kWh) | Total Costs Incurred during the Outage (USD/h) | Total Costs Avoided during the Outage (USD) | Resilience Indices |
|---|---|---|---|---|
| Case 1 | 13,210 | 18,442 | 0 | 0.76 |
| Case 2 | 14,147 | 14,300 | 4141 | 4.42 |
| Case 3 | 14,227 | 11,761 | 6680 | 5.61 |
| Case 4 | 14,040 | 17,717 | 724 | 3.38 |
| Case 5 | 14,173 | 13,473 | 4968 | 4.75 |

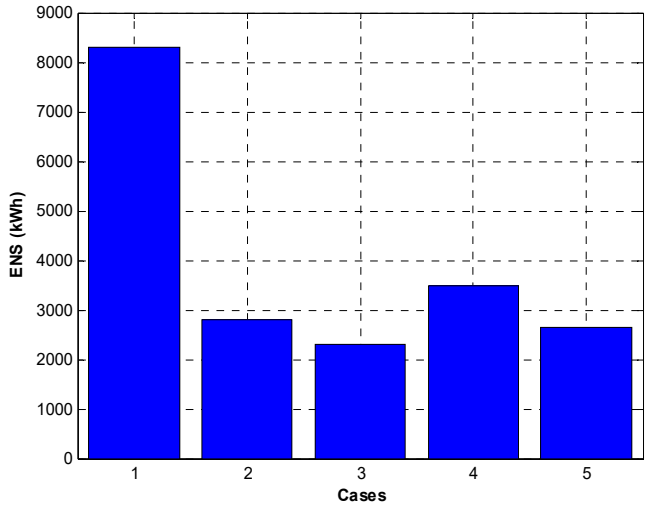


**Figure 11.** Comparison of ENS values under various cases (study I).

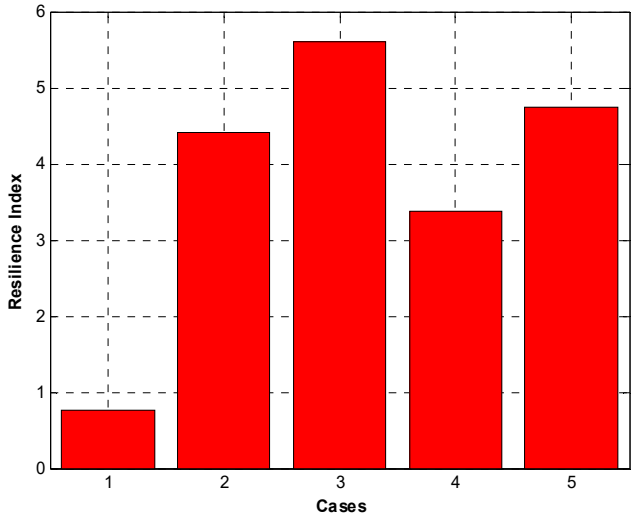


**Figure 12.** Comparison of resilience indices under various cases (study I).

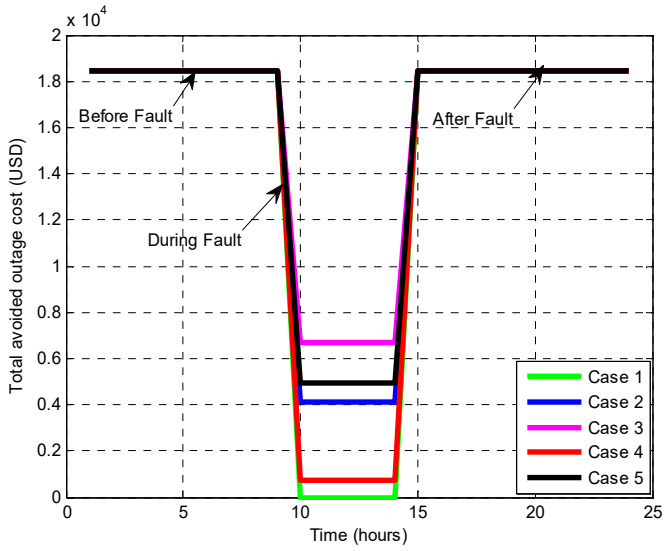


**Figure 13.** Total avoided outage cost (USD) (study I).

### *4.2. Study II (Severe Damage)*

The investigation in case study II focused on a 69-bus RDS, as shown in Figure 14. The primary purpose of this study was to assess the efficacy of both traditional DERs and EMGs in improving the RDS resilience in the case of natural disasters. The simulation simulated the aftermath of a powerful storm, assuming a damaging event along the critical main feeder branch 1–2, which is illustrated in Figure 14. The precise event occurred at 10 a.m., and its duration resulted in a 4 h outage that lasted until 2 p.m. Four unique test cases were used to thoroughly analyze the system's reaction under these adverse situations. These instances were intended to assess the performance and effectiveness of the EMGs and DERs in reducing the impact of the disaster on the resilience of the RDS. During the experiments, we evaluated how the integration of EMGs and DERs aided in managing the power outages, enhancing the system stability, and reducing the downtime. This assessment enabled us to identify the strengths and weaknesses of our RDS and the implemented technologies, providing valuable insights for future enhancements and planning strategies aimed at improving the overall resilience of electrical RDS to natural disasters. Through this process, we aimed to develop a deeper understanding of the effectiveness of EMGs and DERs in mitigating the impact of disruptions and enhancing the reliability of the electrical grid, fostering more resilient and adaptive systems for the future. Additionally, we analyzed how these integrated systems contribute to minimizing downtime and improving system stability, thereby informing our strategies for optimizing resilience in the face of adverse conditions.

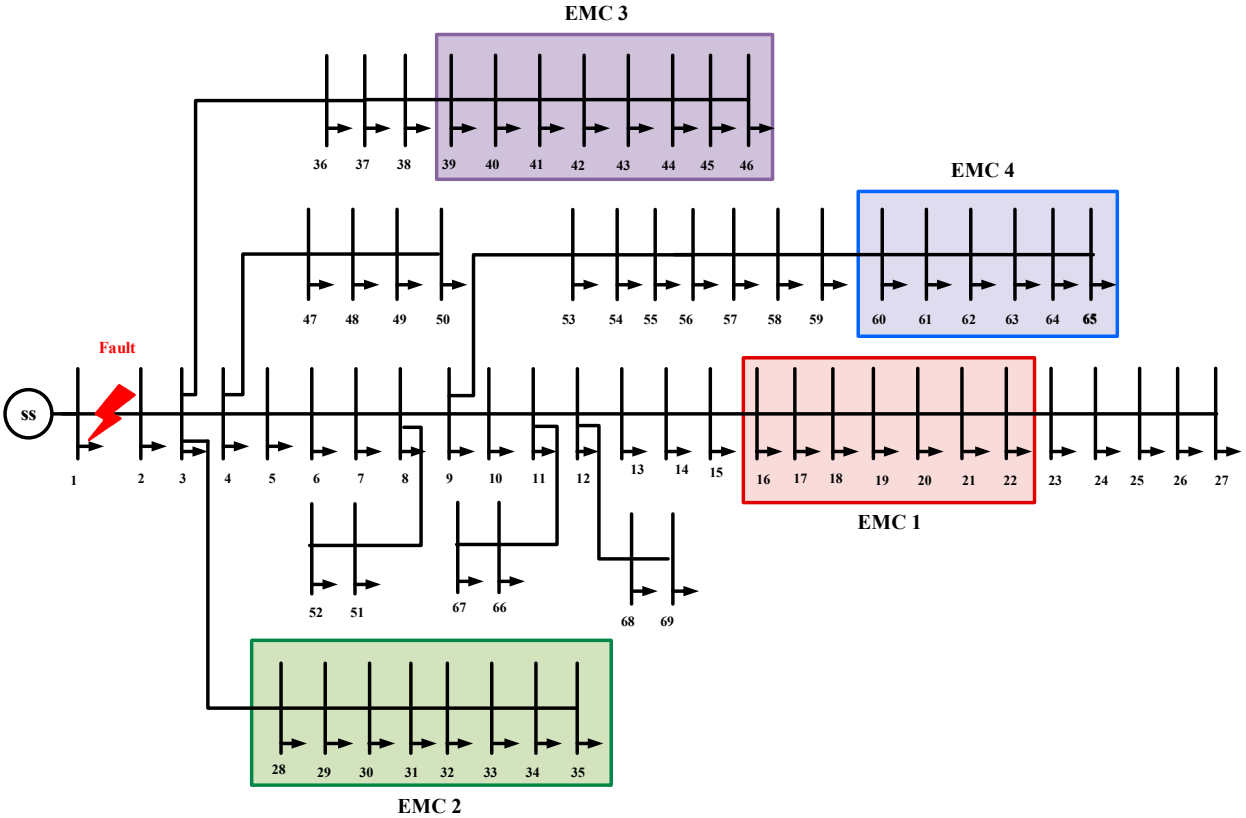


**Figure 14.** IEEE 69-bus RDS without any DERs (study II).

#### 4.2.1. Without Any DERs

The base case assumed that the electricity RDS was not coupled with any DERs. The IEEE 69-bus test system operated on a typical grid in this configuration. This base case simulation, however, encountered various difficulties during the day, particularly at 10 a.m., when four independent faults arose. As seen in Figure 14, these issues caused a 4 h outage that affected all RDS buses. As a result of these problems, a significant percentage of

the load, nearly 3801 kW, was impacted. This study of the base case performance revealed concerning findings, particularly in terms of the ENS value, which rose to a concerning 8292 kWh (Figure 14). This very high ENS indicated a severe energy shortfall during the outage, posing significant hurdles to the system's ability to satisfy demand and maintain operations during critical moments. Furthermore, the RI value was depressingly low at zero. The absence of a backup unit in the system was primarily responsible for the system's zero resilience value. Without a reliable backup, the entire load was vulnerable to faults, leading to a loss of grid supplies. This vulnerability raised significant concerns about potential interruptions and jeopardized the system's overall reliability. Having a backup unit in place is crucial for ensuring continuity of power supply during emergencies and disruptions, thus mitigating the impact of faults and enhancing the system's resilience against unforeseen events.

#### 4.2.2. Clear Day with DERs

The resilience problem was overcome in this example if the weather conditions were those of a clear day. Similar to case study I, the output power of the SPV and WT is obtained from Table 2. In Figure 14, four EMGs are depicted by dotted lines in case study II. The system could partially recover power losses suffered during outages by installing BEVs at the DERs. Figure 15 illustrates the integration of DERs into all EMGs on the IEEE 69-bus RDS. Upon the introduction of DERs in the 69-bus system, the RI increased to 0.56, but the ENS value reduced to 9716 kWh. These gains imply that the system's resilience improved as a result of the allocation of DERs to the EMGs.

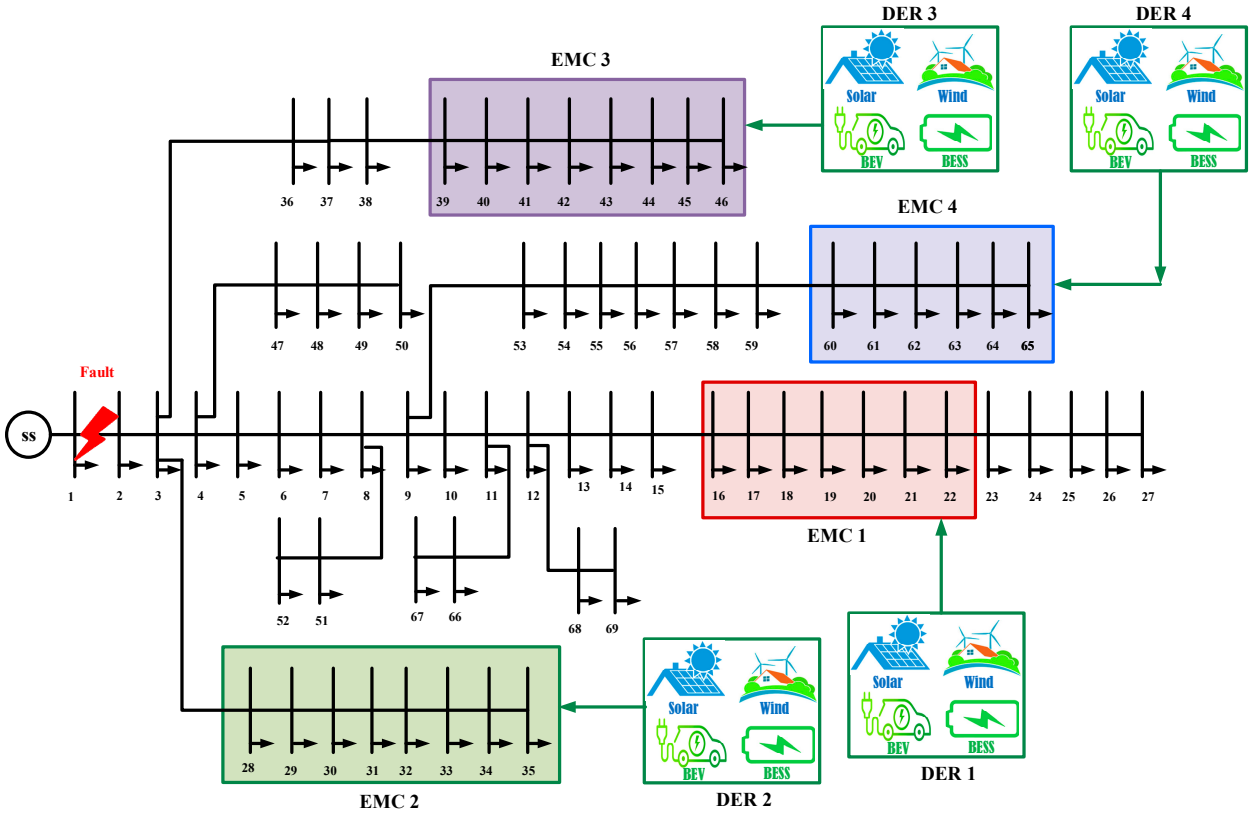


**Figure 15.** IEEE 69-bus RDS with DERs (study II).

#### 4.2.3. Cloudy Day with DERs

In this case, the resilience enhancement problem was solved by assuming overcast weather conditions and taking DERs into account in the RDS. The restoration plan was enacted at 10 a.m., kicking off a 4 h procedure that lasted until 2 p.m. DERs were carefully deployed in the EMG over this period, resulting in a significant reduction in the ENS value

from 15,204 kWh (case 1) to 9218 kWh. Furthermore, the introduction of DERs resulted in a significant decrease in the percentages of affected households, with just 691 (53.92%) having power outages and an average of 12.77% affected, suggesting a major increase in the overall service reliability.

One of the most important effects of this restoration endeavor was an increase in the system's RI, which rose to 0.65. This increase in resilience reflected the system's enhanced ability to tolerate and recover from interruptions, resulting in a more robust and reliable power supply in the face of difficulties. The successful implementation of the restoration plan, as well as the smart deployment of DERs, played critical roles in reducing power outages and increasing the overall grid performance. This accomplishment is a key step toward constructing a more resilient and efficient energy infrastructure that will benefit both consumers and companies.

#### 4.2.4. Rainy Day with DERs

In this case, the optimal position problem was solved by considering rainy weather circumstances. The inclusion of DERs into EMGs had a significant positive impact on the overall system performance. The remarkable resilience index score of 0.46, which shows the system's improved ability to tolerate and recover from disturbances or potential disruptions, is a major signal of this development. This significant improvement was the direct outcome of allocating DERs to EMGs. Furthermore, the decrease in the ENS value to 10,386 kWh supports the notion of greater system resilience. A lower ENS number indicates that less energy demand was unmet during important events or poor conditions, highlighting the efficacy of DERs in improving system reliability. Tables 9 and 10 indicate an intriguing observation: on rainy days, the resilience values were noticeably lower, while the ENS values were greater than on clear and overcast days. This implies that the system's performance during bad weather could still benefit from additional upgrades and specialized measures, although the installation of DERs was shown to be especially beneficial in improving the system's reaction during other weather situations.

**Table 9.** Resilience metrics for electrical utility (study II) of IEEE 69-bus system.

| Cases | Number of Hours of Outage for Total Households (h) | ENS to All Households (kWh) | Total Number and Percentage of Households Impacted | Average Number and Percentage of Households Impacted |
|---|---|---|---|---|
| Case 1 | 5408 | 15,204 | 1352 (100%) | 338 (25%) |
| Case 2 | 2916 | 9716 | 729 (53.92%) | 182.25 (13.48%) |
| Case 3 | 2764 | 9218 | 691 (51.11%) | 172.75 (12.77%) |
| Case 4 | 3116 | 10,386 | 779 (57.62%) | 194.75 (14.4%) |
| Case 5 | 2864 | 9554 | 716 (52.96%) | 179 (13.24%) |

**Table 10.** Cost analysis for resilience metrics (study II) of IEEE 69-bus system.

| Cases | Total Revenue Loss for Utilities (USD/kWh) | Total Costs Incurred during the Outage (USD/h) | Total Costs Avoided during the Outage (USD) | Resilience Indices |
|---|---|---|---|---|
| Case 1 | 12,163 | 77,540 | 0 | 0 |
| Case 2 | 13,041 | 49,552 | 27,989 | 0.56 |
| Case 3 | 13,121 | 47,012 | 30,529 | 0.65 |
| Case 4 | 12,934 | 52,969 | 24,572 | 0.46 |
| Case 5 | 13,067 | 48,724 | 28,816 | 0.59 |

#### 4.2.5. Sunny Day with DERs

In the scenario of a sunny day with DERs, the optimal position problem was addressed, taking into account sunny weather conditions. The remarkable resilience index score of 0.59 reflected a significant improvement in the system's ability to tolerate and recover from

disturbances or potential disruptions. This improvement was directly attributed to the allocation of DERs to EMGs. Furthermore, the decrease in the ENS value to 10,386 kWh indicates greater system resilience. A lower ENS value signifies that less energy demand went unmet during critical events or adverse conditions, underscoring the efficacy of DERs in enhancing the system reliability. Tables 9 and 10 highlight an intriguing observation: on rainy days, the resilience values were notably lower, while the ENS values were higher compared with clear and overcast days. This suggests that the system's performance during inclement weather could still benefit from additional upgrades and specialized measures, despite the demonstrated benefits of installing DERs in improving the system's response during other weather conditions.

In study II, the ENS profiles presented in Figure 16a–e offer valuable insights into the resilience dynamics of the system under various scenarios. Initially, in case 1 without any modifications, the high ENS value of 15,204 kWh indicates a significant level of unmet energy demand during the outages, reflecting the system's vulnerability to disruptions. However, as modifications were introduced in cases 2 through 5, such as improvements in infrastructure or the implementation of enhanced operational strategies, the ENS values consistently decreased. This reduction signifies a more effective mitigation of energy demand during disruptions, indicating an improvement in the system's ability to maintain service continuity, even under adverse conditions. Notably, case 3 stood out with the lowest ENS value of 9218 kWh, suggesting that the implemented modifications in this scenario resulted in the most significant enhancement of system resilience among all cases considered. Overall, these findings underscore the importance of proactive resilience measures in bolstering system reliability and ensuring uninterrupted service delivery during outages and adverse events.

Table 9 presents resilience metrics for the electrical utility performance in study II of the IEEE 69-bus system, providing crucial insights into the system's ability to withstand and recover from disruptions. These metrics, including the number of hours of outage for total households, ENS to all households, total number and percentage of households impacted, and average number and percentage of households impacted, offer a comprehensive overview of the system's resilience under various scenarios. Case 1 demonstrated the highest outage duration, where it impacted all households and resulted in a substantial ENS value of 15,204 kWh. In contrast, case 3 showcased the lowest outage duration, where it affected 51.11% of households, with a significantly lower ENS value of 9218 kWh. This indicates that case 3 exhibited superior resilience performance compared with the others, with fewer households impacted and less energy demand left unmet during outages.

Table 10 delves into the cost analysis for resilience metrics in study II, shedding light on the economic implications of outage events. The metrics included total revenue loss for utilities, total costs incurred during the outage, total costs avoided during the outage, and RI. Notably, case 3 stood out with the highest resilience index of 0.65, indicating its superior performance in minimizing revenue loss and costs during outages compared with other cases. This highlights the effectiveness of the resilience strategies implemented in case 3, which not only reduced the outage durations but also mitigated financial losses for utilities, ultimately enhancing the overall reliability and economic viability of the RDS.

Figures 17 and 18 present a comprehensive comparison of ENS values and RI across different settings of the IEEE 69-bus system. Notably, case 3 consistently exhibited the lowest ENS values and the highest RI compared with the other scenarios analyzed. These data strongly support the effectiveness of the proposed framework in strategically allocating DERs during overcast days, thereby significantly enhancing the resilience of the IEEE 69-bus RDS. The substantial improvements observed in case 3 were particularly encouraging, highlighting the success of the DER allocation strategy in strengthening the system's capacity to withstand and recover from disruptive events, consequently elevating its overall resilience. Additionally, Figure 19 illustrates the total averted outage cost for the RDS before, during, and after the occurrence of disruptive events. Case 3 emerged as the most advantageous scenario, demonstrating a superior total averted outage cost compared

with the other evaluated cases. This outcome reinforced the argument for the proposed framework's effectiveness in enhancing the overall economic performance and reliability of the IEEE 69-bus RDS.

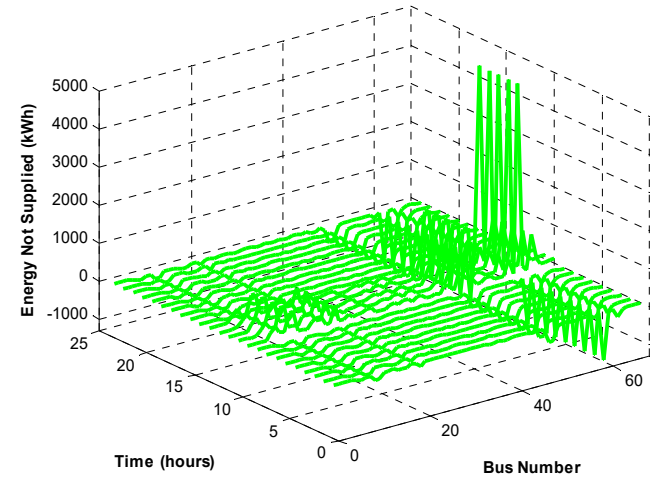


(**a**)

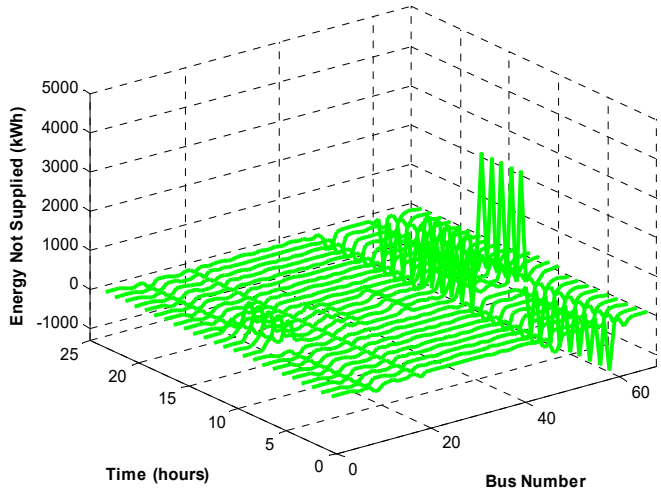


(**b**)

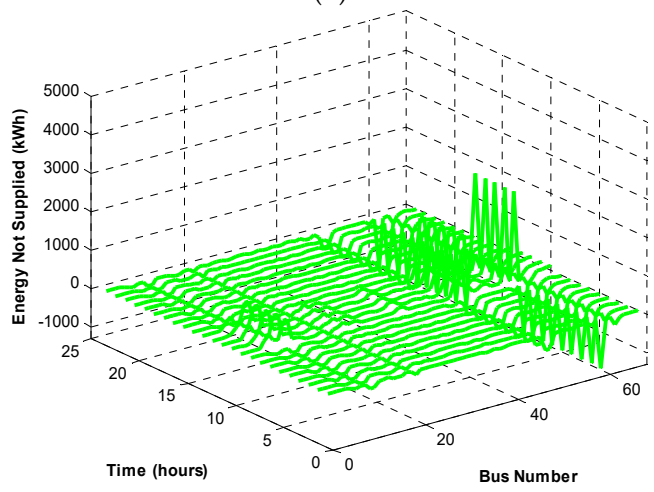


(**c**)

**Figure 16.** *Cont.*

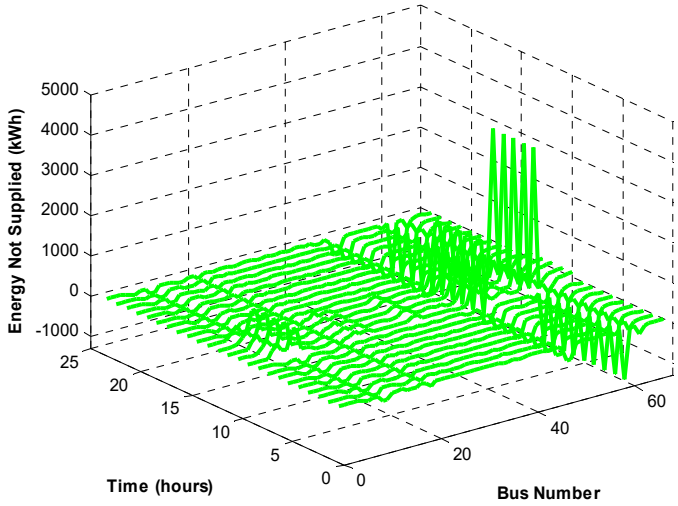


(**d**)

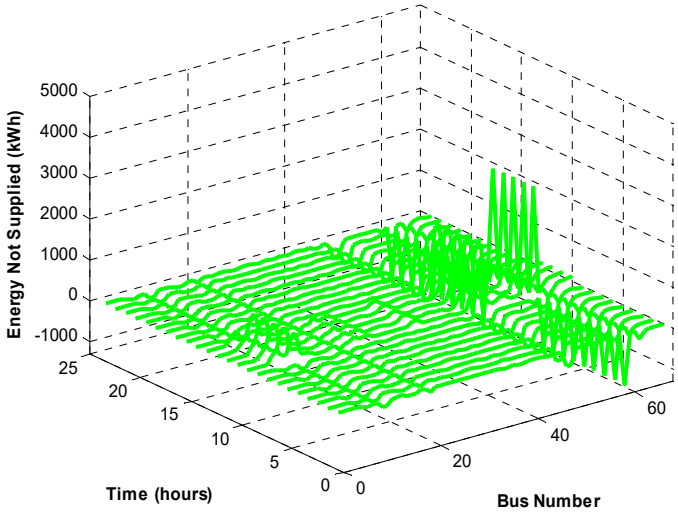


(**e**)

**Figure 16.** (**a**) ENS profile of case I (without any DERs, study II); (**b**) ENS profile of case II (clear day with DERs, study II); (**c**) ENS profile of case III (cloudy day with DERs, study II); (**d**) ENS profile of case IV (rainy day with DERs, study II); (**e**) ENS profile of case V (sunny day with DERs, study II).

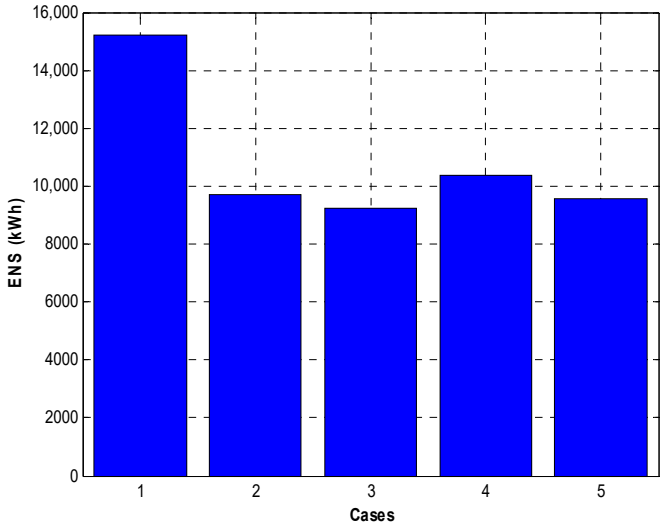


**Figure 17.** Comparison of ENS values under various cases (study II).

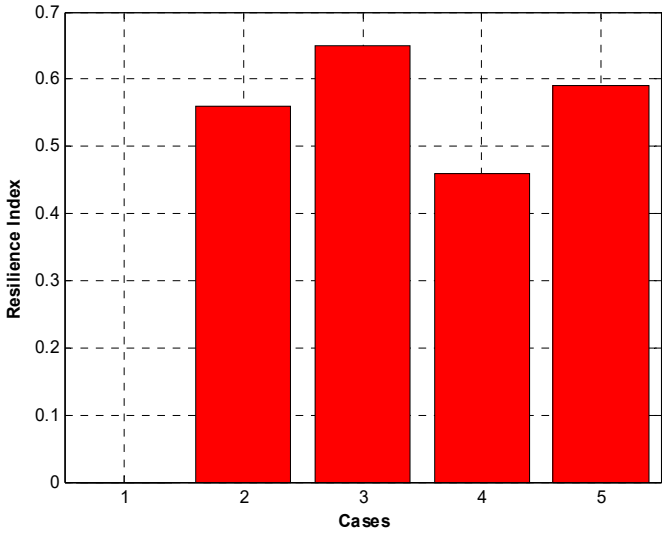


**Figure 18.** Comparison of resilience indices under various cases (study II).

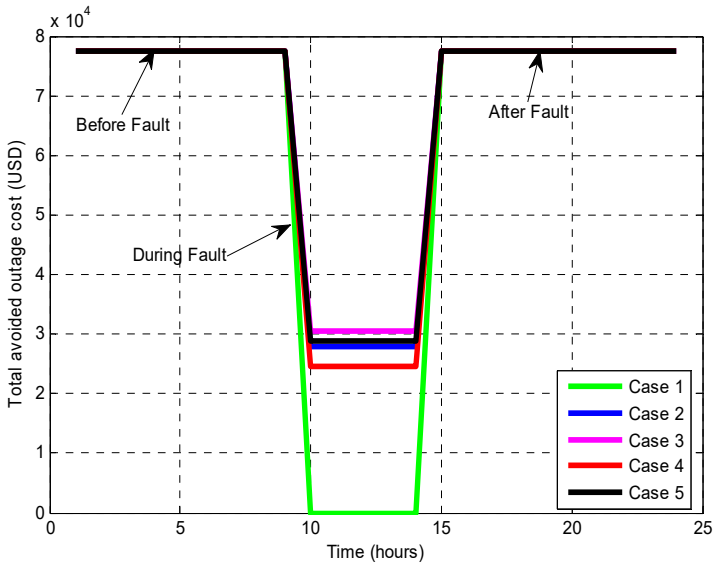


**Figure 19.** Total avoided outage cost (USD) (study II).

### *4.3. Overall Comparative Analysis*

The evaluation of the proposed SMA strategy's effectiveness involved a detailed analysis of its performance within the modified IEEE 69-test system framework. The main aim was to improve the RI and other relevant parameters. A comprehensive comparative analysis was conducted, contrasting the proposed SMA with established algorithms, such as the BESA [29], GSA [40], and ICA [41]. These algorithms were chosen based on their prior application in addressing the resilience improvement challenges within power systems, showcasing their effectiveness in optimizing system resilience. Comparing the proposed SMA with these established algorithms offered a valuable benchmarking opportunity to assess its performance and efficacy in enhancing power system resilience. The analysis was conducted under uniform conditions across both study I, which simulated moderate damage scenarios, and study II, which represented severe damage scenarios. Standardized reference values from the base case served as a basis for comparing the performance of all algorithms, ensuring fair and consistent evaluations.

Table 11 presents data on the DER sizes obtained from different optimization algorithms, reflecting resilience improvement strategies across various weather conditions, including clear days, cloudy days, rainy days, and sunny days. Each case represents a

specific weather condition scenario, and the DER sizes for PV systems, wind turbines, BEVs, and BESSs are listed. These sizes were derived from optimization algorithms, such as SMA, BESA, GSA, and ICA, providing insights into how each algorithm performs in optimizing DER sizes to enhance resilience under different weather conditions.

**Table 11.** Simulation data of DER size for various cases using various algorithms.

| Case | Components | SMA | BESA [29] | GSA [40] | ICA [41] |
|---|---|---|---|---|---|
| Case 2 | Solar PV (kW) | 695 | 650 | 620 | 635 |
| | Wind turbine (kW) | 252 | 228 | 218 | 207 |
| | BEV (kW) | 650 | 580 | 550 | 570 |
| | BESS (kW) | 535 | 490 | 460 | 445 |
| | Total DER size (kW) | 2132 | 1948 | 1848 | 1857 |
| Case 3 | Solar PV (kW) | 348 | 325 | 310 | 318 |
| | Wind turbine (kW) | 870 | 760 | 725 | 690 |
| | BEV (kW) | 650 | 580 | 550 | 570 |
| | BESS (kW) | 535 | 490 | 460 | 445 |
| | Total DER size (kW) | 2403 | 2155 | 2045 | 2023 |
| Case 4 | Solar PV (kW) | 209 | 195 | 186 | 191 |
| | Wind turbine (kW) | 435 | 380 | 363 | 345 |
| | BEV (kW) | 650 | 580 | 550 | 570 |
| | BESS (kW) | 535 | 490 | 460 | 445 |
| | Total DER size (kW) | 1829 | 1645 | 1559 | 1551 |
| Case 5 | Solar PV (kW) | 544 | 488 | 465 | 476 |
| | Wind turbine (kW) | 522 | 456 | 435 | 414 |
| | BEV (kW) | 650 | 580 | 550 | 570 |
| | BESS (kW) | 535 | 490 | 460 | 445 |
| | Total DER size (kW) | 2251 | 2014 | 1910 | 1905 |

The outcomes of each optimization method were meticulously documented and are presented in Tables 12 and 13, offering a comprehensive overview of the results obtained from each algorithm for studies I and II. These tables facilitate a direct comparison of their performance across various resilience metrics. Remarkably, the findings consistently indicate that the SMA outperformed its counterparts across all studies and cases.

**Table 12.** Comparison of various resilience parameters using various algorithms (study I).

| Case | Resilience Metrics | SMA | BESA [29] | GSA [40] | ICA [41] |
|---|---|---|---|---|---|
| Case 2 | Number of hours of outage for total households (h) | 840 | 888 | 954 | 902 |
| | ENS to all households (kWh) | 2804 | 2960 | 3180 | 3008 |
| | Total number and percentage of households impacted | 210 (15.53%) | 222 (16.42%) | 239 (17.64%) | 226 (16.68%) |
| | Average number and percentage of households impacted | 52.5 (3.8%) | 55.5 (4.1%) | 59.62 (4.41%) | 56.4 (4.17%) |
| | Total revenue loss for utilities (USD/kWh) | 14,147 | 14,122 | 14,087 | 14,115 |
| | Total costs incurred during the outage (USD/h) | 14,300 | 15,096 | 16,218 | 15,341 |
| | Total costs avoided during the outage (USD) | 4141 | 3346 | 2223 | 3101 |
| | Resilience indices | 4.42 | 4.14 | 3.78 | 4.05 |

**Table 12.** *Cont.*

| Case | Resilience Metrics | SMA | BESA [29] | GSA [40] | ICA [41] |
|---|---|---|---|---|---|
| Case 3 | Number of hours of outage for total households (h) | 692 | 719 | 751 | 725 |
| | ENS to all households (kWh) | 2306 | 2398 | 2502 | 2416 |
| | Total number and percentage of households impacted | 173 (12.79%) | 180 (13.3%) | 188 (13.87%) | 181 (13.41%) |
| | Average number and percentage of households impacted | 43.25 (3.19%) | 45 (3.33%) | 46.91 (3.47%) | 45.3 (3.35%) |
| | Total revenue loss for utilities (USD/kWh) | 14,227 | 14,212 | 14,196 | 14,209 |
| | Total costs incurred during the outage (USD/h) | 11,761 | 12,230 | 12,760 | 12,322 |
| | Total costs avoided during the outage (USD) | 6680 | 6211 | 5681 | 6120 |
| | Resilience indices | 5.61 | 5.34 | 5.08 | 5.29 |
| Case 4 | Number of hours of outage for total households (h) | 1044 | 1076 | 1093 | 1086 |
| | ENS to all households (kWh) | 3474 | 3588 | 3642 | 3620 |
| | Total number and percentage of households impacted | 261 (19.30%) | 269 (19.90%) | 273 (20.20%) | 271 (20.08%) |
| | Average number and percentage of households impacted | 62.25 (4.82%) | 67.27 (4.98%) | 68.28 (5.05%) | 67.87 (5.02%) |
| | Total revenue loss for utilities (USD/kWh) | 14,040 | 14,022 | 14,013 | 14,017 |
| | Total costs incurred during the outage (USD/h) | 17,717 | 18,299 | 18,574 | 18,462 |
| | Total costs avoided during the outage (USD) | 724 | 142.8 | 132 | 20.4 |
| | Resilience indices | 3.38 | 3.23 | 3.17 | 3.2 |
| Case 5 | Number of hours of outage for total households (h) | 792 | 811 | 839 | 823 |
| | ENS to all households (kWh) | 2642 | 2702 | 2796 | 2744 |
| | Total number and percentage of households impacted | 198 (14.64%) | 202 (14.98%) | 210 (15.51%) | 206 (15.22%) |
| | Average number and percentage of households impacted | 49.5 (3.66%) | 50.5 (3.74%) | 52.42 (3.87%) | 51.45 (3.81%) |
| | Total revenue loss for utilities (USD/kWh) | 14,173 | 14,164 | 14,148 | 14,157 |
| | Total costs incurred during the outage (USD/h) | 13,473 | 13,780 | 14,260 | 13,994 |
| | Total costs avoided during the outage (USD) | 4968 | 4661 | 4182 | 4447 |
| | Resilience indices | 4.75 | 4.63 | 4.44 | 4.54 |

**Table 13.** Comparison of various resilience parameters using various algorithms (study II).

| Case | Resilience Metrics | SMA | BESA [29] | GSA [40] | ICA [41] |
|---|---|---|---|---|---|
| Case 2 | Number of hours of outage for total households (h) | 2916 | 2962 | 3028 | 2976 |
| | ENS to all households (kWh) | 9716 | 9872 | 10,092 | 9920 |
| | Total number and percentage of households impacted | 729 (53.92%) | 740 (54.76%) | 757 (55.98%) | 744 (55.03%) |
| | Average number and percentage of households impacted | 182.25 (13.48%) | 185 (13.69%) | 189.22 (13.99%) | 186 (13.75%) |
| | Total revenue loss for utilities (USD/kWh) | 13,041 | 13,016 | 12,981 | 13,009 |
| | Total costs incurred during the outage (USD/h) | 49,552 | 50,347 | 51,469 | 50,592 |
| | Total costs avoided during the outage (USD) | 27,989 | 27,193 | 26,071 | 26,948 |
| | Resilience indices | 0.56 | 0.54 | 0.51 | 0.53 |
| Case 3 | Number of hours of outage for total households (h) | 2764 | 2793 | 28,242 | 2798 |
| | ENS to all households (kWh) | 9218 | 9310 | 9414 | 9328 |
| | Total number and percentage of households impacted | 691 (51.11%) | 698 (51.65%) | 706 (52.22%) | 700 (51.75%) |
| | Average number and percentage of households impacted | 172.75 (12.77%) | 174.56 (12.91%) | 176.51 (13.06%) | 174.90 (12.94%) |
| | Total revenue loss for utilities (USD/kWh) | 13,121 | 13,106 | 13,090 | 13,103 |
| | Total costs incurred during the outage (USD/h) | 47,012 | 47,481 | 48,011 | 47,573 |
| | Total costs avoided during the outage (USD) | 30,529 | 30,059 | 29,529 | 29,968 |
| | Resilience indices | 0.65 | 0.63 | 0.61 | 0.62 |
| Case 4 | Number of hours of outage for total households (h) | 3116 | 3150 | 3166 | 3159 |
| | ENS to all households (kWh) | 10,386 | 10,500 | 10,554 | 10,532 |
| | Total number and percentage of households impacted | 779 (57.62%) | 788 (58.24%) | 792 (58.55%) | 790 (58.42%) |
| | Average number and percentage of households impacted | 194.75 (14.4%) | 196.87 (14.56%) | 197.88 (14.63%) | 197.47 (14.60%) |
| | Total revenue loss for utilities (USD/kWh) | 12,934 | 12,916 | 12,907 | 12,911 |
| | Total costs incurred during the outage (USD/h) | 52,969 | 53,550 | 53,825 | 53,713 |
| | Total costs avoided during the outage (USD) | 24,572 | 23,990 | 23,715 | 23,827 |
| | Resilience indices | 0.46 | 0.45 | 0.44 | 0.44 |

**Table 13.** *Cont.*

| Case | Resilience Metrics | SMA | BESA [29] | GSA [40] | ICA [41] |
|---|---|---|---|---|---|
| Case 5 | Number of hours of outage for total households (h) | 2864 | 2884 | 2912 | 2897 |
| | ENS to all households (kWh) | 9554 | 9614 | 9708 | 9656 |
| | Total number and percentage of households impacted | 716 (52.96%) | 721 (53.33%) | 728 (53.85%) | 724 (53.56%) |
| | Average number and percentage of households impacted | 179 (13.24%) | 180.26 (13.33%) | 182.02 (13.46%) | 181.05 (13.39%) |
| | Total revenue loss for utilities (USD/kWh) | 13,067 | 13,058 | 13,043 | 13,051 |
| | Total costs incurred during the outage (USD/h) | 48,724 | 49,031 | 49,511 | 49,246 |
| | Total costs avoided during the outage (USD) | 28,816 | 28,509 | 28,030 | 28,295 |
| | Resilience indices | 0.59 | 0.58 | 0.56 | 0.57 |

The superiority of the SMA was particularly evident in its ability to optimize the allocation of DER and BEV effectively. This optimization contributed significantly to bolstering the RI, thereby enhancing the overall resilience of the system. The consistent trend observed across all studies and cases solidified the position of SMA as the preferred approach for optimizing DER and BEV allocation in scenarios aimed at improving system resilience. In essence, the evaluation underscored the robustness and effectiveness of the SMA strategy in enhancing system resilience across diverse conditions. Its superior performance, as evidenced by the comparative analysis, highlights its potential to serve as a valuable tool in mitigating the impacts of disruptions and ensuring the reliability of critical infrastructure.

Throughout the comparative analysis conducted in this study, the SMA consistently emerged as the superior choice in assessing system resilience, as evidenced by its numerical values for resilience parameters. In each case examined, the SMA consistently predicted lower ENS values and higher RIs compared with the alternative algorithms, such as the BESA, GA, and ICA. This consistent trend underscores the robustness and reliability of the SMA in capturing the intricate dynamics of system resilience across diverse outage scenarios.

For instance, in case 2, where the SMA estimated an ENS of 2804 kWh, it significantly outperformed alternative algorithms, which yielded values ranging from 2960 kWh to 3180 kWh. Similarly, in case 3, the SMA's prediction of an ENS of 2306 kWh surpassed the range of values obtained from alternative algorithms, which ranged from 2398 kWh to 2502 kWh. Notably, this pattern persisted across cases 4 and 5, with the SMA consistently providing lower ENS values and higher RIs compared with the alternative algorithms.

Furthermore, Figures 20 and 21 enriches the analysis by providing visual representations of the comparative assessment conducted in study I. Figure 20 illustrates the comparison of ENS values using various algorithms, highlighting differences in ENS to households across different outage scenarios. Conversely, Figure 21 visually demonstrates the comparison of RIs using various algorithms, showcasing variations in system resilience, as assessed by different algorithms. Overall, the insights derived from Table 12, coupled with Figures 20 and 21, underscored the consistent superiority of the SMA in evaluating system resilience across diverse outage scenarios in study I.

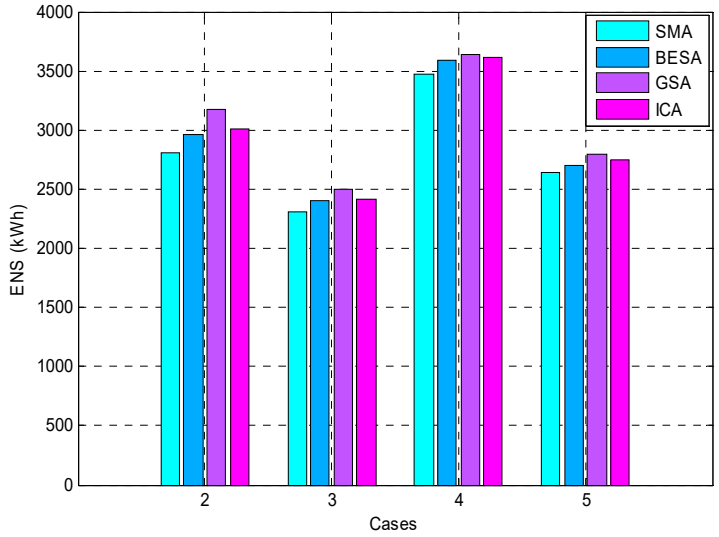


**Figure 20.** Comparison of ENS values found by employing various algorithms (study I).

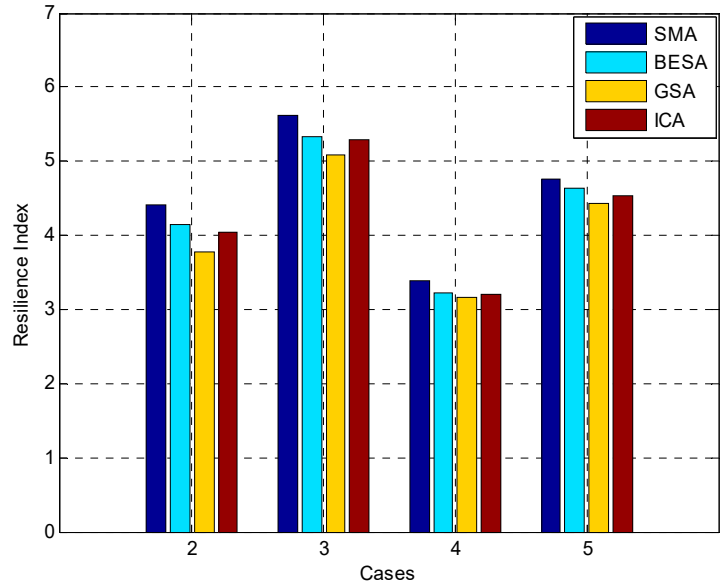


**Figure 21.** Comparison of resilience indices found by employing various algorithms (study I).

These precise numerical comparisons highlight the consistent superiority of the SMA in assessing system resilience, reaffirming its effectiveness and reliability in real-world applications. By offering a comprehensive understanding of the SMA's performance across various outage scenarios, this study underscored its potential as a valuable tool for decision makers and stakeholders in enhancing the resilience of critical systems and infrastructure.

Table 13 offers an extensive comparison of various resilience parameters by utilizing different algorithms in study II, providing crucial insights into the system's robustness and adaptability across diverse outage scenarios. This comprehensive analysis encompassed metrics such as the number of outage hours for total households, ENS to all households, total and average number of impacted households, revenue loss for utilities, total costs incurred and avoided during outages, and RI for each case studied. In case 2, the SMA predicted 2916 h of outage for total households, accompanied by an ENS of 9716 kWh. Notably, the SMA demonstrated superior performance with a resilience index of 0.56 compared with the alternative algorithms, namely, BESA, GSA, and ICA, which yielded RIs of 0.54, 0.51, and 0.53, respectively. Transitioning to case 3, the SMA estimated 2764 outage hours and an ENS of 9218 kWh, resulting in an impressive resilience index of 0.65. This surpassed the RI obtained from alternative algorithms, emphasizing the SMA's

efficacy in assessing the system resilience. Moving forward, case 4 showcased the SMA predicting 3116 outage hours and an ENS of 10,386 kWh, with a resilience index of 0.46, which outperformed alternative algorithms in the resilience assessment. Lastly, in case 5, the SMA estimated 2864 outage hours and an ENS of 9554 kWh, yielding a resilience index of 0.59, further demonstrating its superiority over other algorithms. Furthermore, Figures 17 and 18 enhanced the analysis by offering visual representations of the comparative assessment conducted in study II. Figure 22 depicted the comparison of ENS values using various algorithms, illustrating differences in the ENS to households across different outage scenarios. Conversely, Figure 23 visually demonstrated the comparison of RIs using various algorithms, highlighting variations in the system resilience, as assessed by different algorithms. Overall, the insights gleaned from Table 13, coupled with Figures 22 and 23, underscored the consistent superiority of the SMA in evaluating the system resilience across diverse outage scenarios in study II.

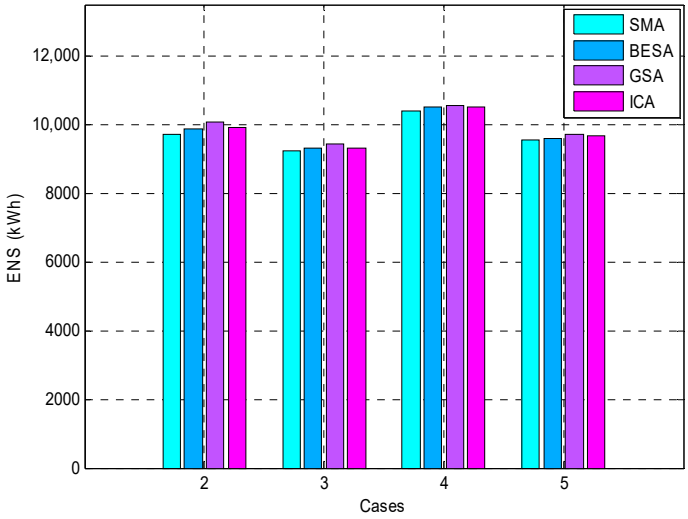


**Figure 22.** Comparison of ENS values found by employing various algorithms (study II).

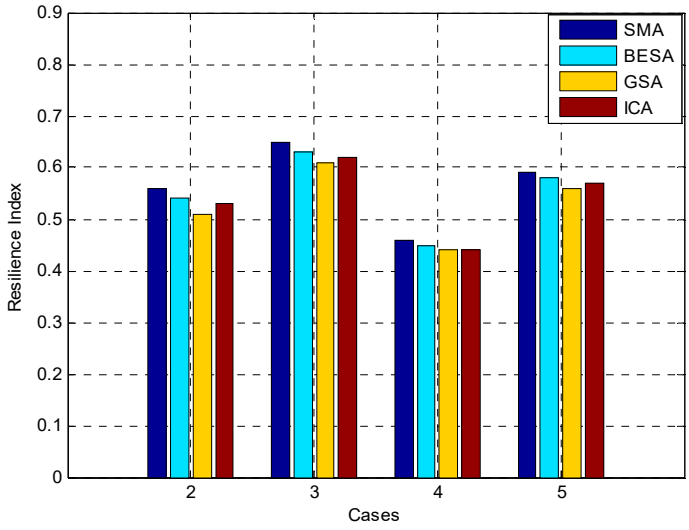


**Figure 23.** Comparison of resilience indices found by employing various algorithms (study II).

### *4.4. Overall Outcome*

The examination of weather conditions (clear, cloudy, rainy, and sunny) across two case studies revealed that case 3 presented the most effective strategy for enhancing resilience. Throughout all the case studies, the simulation results consistently showed that case 3, particularly on cloudy days, exhibited the lowest ENS values and the highest RI. This

approach yielded more realistic outcomes by considering a range of weather conditions rather than relying solely on ideal weather scenarios, such as clear days or constant wind speeds. The proposed methodology ensured adaptability regardless of weather conditions, thereby facilitating more efficient RDS planning through the optimal utilization of intermittent DERs and BEVs. The significance of this research lies in the benefits it provides to distribution operators and utilities during the RDS expansion planning phase. They can leverage the proposed method to identify the most cost-effective locations for deploying new or future DER facilities. This optimization in site selection results in a more robust and resilient RDS that is better equipped to address various weather-related challenges and uncertainties. The findings of this study underscore the importance of considering diverse weather conditions when planning an RDS and demonstrate how the proposed approach optimizes the utilization of intermittent DERs and BEVs, leading to improved resilience and cost-effectiveness. This study has the potential to revolutionize the way RDSs are planned and operated, delivering significant advantages to both operators and consumers.

### *4.5. Addressing Policy Implications*

Understanding the policy implications of research findings is crucial for ensuring the scientific advancements translate into meaningful real-world impact. In the context of distribution system resilience and extreme weather events, policymakers and stakeholders require insights into how the proposed solutions align with existing policies, regulations, and initiatives, as well as opportunities for policy innovation and improvement. Therefore, this study not only investigates technical aspects but also examines the policy landscape surrounding distribution system resilience.

#### 4.5.1. Policy Contextualization

The current policy landscape related to distribution system resilience and extreme weather events is characterized by various policies, regulations, and initiatives aimed at enhancing grid resilience and promoting the integration of DERs and BEVs. These policies often prioritize objectives such as grid reliability, the reduction of greenhouse gas emissions, and the promotion of energy independence.

#### 4.5.2. Policy Alignment

The proposed approach, which leverages prosumer-centric microgrids with integrated DERs and BEVs, closely aligns with the objectives and goals of existing policies and initiatives. By enhancing grid resilience and promoting the use of renewable energy sources, this approach contributes to the overarching goal of enhancing energy security and reducing the environmental impact. Additionally, the emphasis on decentralized energy generation and storage supports the transition toward a more resilient and sustainable energy system.

#### 4.5.3. Policy Recommendations

Based on the research findings and analysis, several policy recommendations are proposed to support the adoption and deployment of prosumer-centric microgrids. These recommendations include updating regulatory frameworks to facilitate grid interconnection of microgrids, developing new incentive programs to encourage investment in DERs and EVs, and establishing resilience planning guidelines to promote stakeholder collaboration and coordination. Implementing these recommendations can create an enabling environment for the widespread adoption of the proposed approach and enhance the resilience of distribution systems to extreme weather events.

#### 4.5.4. Policy Challenges and Opportunities

It is important to acknowledge several challenges and opportunities associated with implementing the proposed approach within the current policy context, including regulatory barriers, financing constraints, and technological limitations. However, there are

also opportunities for policy innovation and collaboration, such as exploring new financing mechanisms and leveraging emerging technologies to overcome these challenges and accelerate the transition toward a more resilient energy system.

#### 4.5.5. Stakeholder Engagement

Active engagement with policymakers, regulators, industry stakeholders, and community organizations throughout the research process was instrumental in gathering input and feedback on the findings and recommendations. This stakeholder engagement process shaped the policy recommendations and ensured their relevance and feasibility. Continued stakeholder engagement is essential to facilitate the effective implementation of the proposed approach and drive positive change in the energy sector. By addressing policy implications, this study aimed to provide policymakers and stakeholders with actionable insights to inform policy decisions and drive progress toward a more resilient energy future.

## 5. Conclusions

In this research, the potential of prosumer-centric microgrids to enhance the resilience and dependability of distribution grids, especially during adverse weather conditions, was highlighted. By integrating various DERs and BEVs into a networked microgrid system, a robust energy infrastructure capable of effectively responding to severe weather events was demonstrated. Through extensive testing on the IEEE 69-bus RDS under diverse weather conditions, this study showcased the microgrid's adaptability and performance. It effectively utilized RES during clear weather and optimized battery storage and DERs during inclement weather to ensure a reliable power supply to critical loads. The inclusion of BEVs as mobile energy storage units proved beneficial for providing backup power during emergencies and enhancing grid stability.

These findings offer valuable insights for policymakers, energy suppliers, and communities in building resilient energy infrastructure. By prioritizing investments in prosumer-centric microgrids and embracing renewable energy initiatives, policymakers can enhance grid resilience and reliability. Energy suppliers can leverage these insights to develop innovative solutions for grid modernization, while communities can explore opportunities for greater engagement in renewable energy projects. With ongoing technological advancements and increased prosumer engagement, a cleaner, more resilient energy future is achievable.

**Author Contributions:** Validation, R.H., T.Y. and N.P.; Formal analysis, M.T. and T.Y.; Writing—original draft, M.T.; Writing—review & editing, N.P.; Supervision, R.H. All authors have read and agreed to the published version of the manuscript.

**Funding:** This research received no external funding.

**Institutional Review Board Statement:** Not applicable.

**Informed Consent Statement:** Not applicable.

**Data Availability Statement:** No new data were created or analyzed in this study. Data sharing is not applicable to this article.

**Acknowledgments:** The authors express their gratitude to the editor and the anonymous reviewers for their valuable feedback and suggestions on an earlier version of this paper, which greatly contributed to its improvement.

**Conflicts of Interest:** The authors declare no conflicts of interest.

## References

1. Jasiūnas, J.; Lund, P.D.; Mikkola, J. Energy system resilience—A review. *Renew. Sustain. Energy Rev.* **2021**, *150*, 111476. [CrossRef]
2. Mujjuni, F.; Betts, T.R.; Blanchard, R.E. Evaluation of Power Systems Resilience to Extreme Weather Events: A Review of Methods and Assumptions. *IEEE Access* **2023**, *11*, 87279–87296. [CrossRef]

3. Gholami, A.; Aminifar, F.; Shahidehpour, M. Front lines against the darkness: Enhancing the resilience of the electricity grid through microgrid facilities. *IEEE Electrif. Mag.* **2016**, *4*, 18–24. [CrossRef]
4. NOAA National Centers for Environmental Information (NCEI). U.S. Billion-Dollar Weather and Climate Disasters. 2024. Available online: https://www.ncei.noaa.gov/access/billions/ (accessed on 12 February 2024).
5. Beyza, J.; Yusta, J.M. Characterising the security of power system topologies through a combined assessment of reliability, robustness, and resilience. *Energy Strategy Rev.* **2022**, *43*, 100944. [CrossRef]
6. Lin, Y.; Bie, Z.; Qiu, A. A review of key strategies in realizing power system resilience. *Glob. Energy Interconnect.* **2018**, *1*, 70–78.
7. Afzal, S.; Mokhlis, H.; Illias, H.A.; Mansor, N.N.; Shareef, H. State-of-the-art review on power system resilience and assessment techniques. *IET Gener. Transm. Distrib.* **2020**, *14*, 6107–6121. [CrossRef]
8. Tabatabaei, N.M.; Ravadanegh, S.N.; Bizon, N. *Power Systems Resilience*; Springer: Cham, Switzerland, 2018.
9. Farzin, H.; Fotuhi-Firuzabad, M.; Moeini-Aghtaie, M. Enhancing power system resilience through hierarchical outage management in multi-microgrids. *IEEE Trans. Smart Grid* **2016**, *7*, 2869–2879. [CrossRef]
10. Che, L.; Shahidehpour, M. DC microgrids: Economic operation and enhancement of resilience by hierarchical control. *IEEE Trans. Smart Grid* **2014**, *5*, 2517–2526.
11. Mousavizadeha, S.; Ghanizadeh Bolandib, T.; Haghifama, M.R.; Moghimic, M.; Luc, J. Resilience analysis of electric distribution networks: A new approach based on modularity concept. *Int. J. Electr. Power Energy Syst.* **2020**, *117*, 105669. [CrossRef]
12. Rosales-Asensio, E.; Martín, M.S.; Borge-Diez, D.; Blanes-Peiro, J.J.; Colmenar-Santos, A. Microgrids with energy storage systems as a means to increase power resilience: An application to office buildings. *Energy* **2019**, *172*, 1005–1015. [CrossRef]
13. Barnes, A.; Nagarajan, H.; Yamangil, E.; Bent, R.; Backhaus, S. Resilient design of largescale distribution feeders with networked microgrids. *Electr. Power Syst. Res.* **2019**, *171*, 150–157. [CrossRef]
14. Zhua, J.; Yuana, Y.; Wang, W. An exact microgrid formation model for load restoration in resilient distribution system. *Int. J. Electr. Power Energy Syst.* **2019**, *116*, 105568. [CrossRef]
15. Ren, L.; Qin, Y.; Li, Y.; Zhang, P.; Wang, B.; Luh, P.B.; Han, S.; Orekan, T.; Gong, T. Enabling resilient distributed power sharing in networked microgrids through software defined networking. *Appl. Energy* **2017**, *210*, 1251–1265. [CrossRef]
16. Shahida, M.U.; Mansoor Khan, M.; Hashmi, K.; Boudina, R.; Khana, A.; Yuning, J.; Tang, H. Renewable energy source (RES) based islanded DC microgrid with enhanced resilient control. *Int. J. Electr. Power Energy Syst.* **2019**, *113*, 461–471. [CrossRef]
17. Hussain, A.; Bui, V.H.; Kim, H.M. Microgrids as a resilience resource and strategies used by microgrids for enhancing resilience. *Appl. Energy* **2019**, *240*, 56–72. [CrossRef]
18. Gilasi, Y.; Hosseini, S.H.; Ranjbar, H. Resiliency-oriented optimal siting and sizing of distributed energy resources in distribution systems. *Electr. Power Syst. Res.* **2022**, *208*, 107875. [CrossRef]
19. Hussain, A.; Ali Shah, S.D.; Muhammad Arif, S. Heuristic optimisation-based sizing and siting of DGs for enhancing resilience of autonomous microgrid networks. *IET Smart Grid* **2019**, *2*, 269–282. [CrossRef]
20. Ghasemi, M.; Kazemi, A.; Bompard, E.; Aminifar, F. A two-stage resilience improvement planning for power distribution systems against hurricanes. *Int. J. Electr. Power Energy Syst.* **2021**, *132*, 107214. [CrossRef]
21. Tari, A.N.; Sepasian, M.S.; Kenari, M.T. Resilience assessment and improvement of distribution networks against extreme weather events. *Int. J. Electr. Power Energy Syst.* **2021**, *125*, 106414. [CrossRef]
22. Amirioun, M.H.; Aminifar, F.; Lesani, H.; Shahidehpour, M. Metrics and quantitative framework for assessing microgrid resilience against windstorms. *Int. J. Electr. Power Energy Syst.* **2019**, *104*, 716–723. [CrossRef]
23. Kayal, P. Resiliency improvement in power distribution infrastructure employing distributed generation and switches—A review summary. *Energy Ecol. Environ.* **2023**, *8*, 195–210. [CrossRef]
24. Li, Z.; Tang, W.; Lian, X.; Chen, X.; Zhang, W.; Qian, T. A resilience-oriented two-stage recovery method for power distribution system considering transportation network. *Int. J. Electr. Power Energy Syst.* **2022**, *135*, 107497. [CrossRef]
25. Li, B.; Chen, Y.; Wei, W.; Huang, S.; Xiong, Y.; Mei, S.; Hou, Y. Routing and scheduling of electric buses for resilient restoration of distribution system. *IEEE Trans. Transp. Electrif.* **2021**, *7*, 2414–2428. [CrossRef]
26. Khomami, M.S.; Jalilpoor, K.; Kenari, M.T.; Sepasian, M.S. Bi-level network reconfiguration model to improve the resilience of distribution systems against extreme weather events. *IET Gener. Transm. Distrib.* **2019**, *13*, 3302–3310. [CrossRef]
27. Dumas, M.; Kc, B.; Cunliff, C.I. *Extreme Weather and Climate Vulnerabilities of the Electric Grid: A Summary of Environmental Sensitivity Quantification Methods*; No. ORNL/TM-2019/1252; Oak Ridge National Lab. (ORNL): Oak Ridge, TN, USA, 2019.
28. Hines, P.; Balasubramaniam, K.; Sanchez, E.C. Cascading failures in power grids. *IEEE Potentials* **2009**, *28*, 24–30. [CrossRef]
29. Yuvaraj, T.; Devabalaji, K.R.; Suresh, T.D.; Prabaharan, N.; Ueda, S.; Senjyu, T. Enhancing Indian Practical Distribution System Resilience Through Microgrid Formation and Integration of Distributed Energy Resources Considering Battery Electric Vehicle. *IEEE Access* **2023**, *11*, 133521–133539. [CrossRef]
30. Li, S.; Chen, H.; Wang, M.; Heidari, A.A.; Mirjalili, S. Slime mould algorithm: A new method for stochastic optimization. *Future Gener. Comput. Syst.* **2020**, *111*, 300–323. [CrossRef]
31. Yuvaraj, T.; Suresh, T.D.; Meyyappan, U.; Aljafari, B.; Thanikanti, S.B. Optimizing the allocation of renewable DGs, DSTATCOM, and BESS to mitigate the impact of electric vehicle charging stations on radial distribution systems. *Heliyon* **2023**, *9*, e23017.
32. Sullivan, M.J.; Schellenberg, J.; Blundell, M. *Updated Value of Service Reliability Estimates for Electric Utility Customers in the United States*; Technical Report; Lawrence Berkeley National Laboratory: Berkeley, CA, USA, 2015.

33. Galvan, E.; Mandal, P.; Sang, Y. Networked microgrids with roof-top solar PV and battery energy storage to improve distribution grids resilience to natural disasters. *Int. J. Electr. Power Energy Syst.* **2020**, *123*, 106239. [CrossRef]
34. U.S. Energy Information Administration. *Average Frequency and Duration of Electric Distribution Outages Vary by States*; Annual Electric Power Industry Report; U.S. Energy Information Administration: Washington, DC, USA, 2023.
35. Sahoo, N.C.; Prasad, K. A fuzzy genetic approach for network reconfiguration to enhance voltage stability in radial distribution systems. *Energy Convers. Manag.* **2006**, *47*, 3288–3306. [CrossRef]
36. InsideEVs.com. Available online: https://insideevs.com/reviews/344001/compare-evs/ (accessed on 30 June 2023).
37. Tesla Motors. Tesla Charging. 2023. Available online: https://www.tesla.com/models-charging#/basics (accessed on 30 June 2023).
38. Tesla Motors. Tesla Powerwall. 2023. Available online: https://www.tesla.com/powerwall (accessed on 30 June 2023).
39. Galvan, E.; Mandal, P.; Chakraborty, S.; Senjyu, T. Efficient energy-management system using a hybrid transactive-model predictive control mechanism for prosumer-centric networked microgrids. *Sustainability* **2019**, *11*, 5436. [CrossRef]
40. Najafi, J.; Peiravi, A.; Anvari-Moghaddam, A.; Guerrero, J.M. Resilience improvement planning of power-water distribution systems with multiple microgrids against hurricanes using clean strategies. *J. Clean. Prod.* **2019**, *223*, 109–126. [CrossRef]
41. Wang, H.; Wang, S.; Yu, L.; Hu, P. A novel planning-attack-reconfiguration method for enhancing resilience of distribution systems considering the whole process of resiliency. *Int. Trans. Electr. Energy Syst.* **2020**, *30*, e12199. [CrossRef]